Neuroimaging for the Neurologist

Clinical MRI and Future Trends

Nandor K. Pinter, MD[a,b], Joseph V. Fritz, PhD[c,d,*]

KEYWORDS

• Neuroimaging • MRI • Emerging MRI techniques

KEY POINTS

- MRI is a versatile technology that continually introduces new methods for visualizing anatomic and physiologic characteristics.
- Neurologists should be sufficiently versed in available and upcoming MRI methods to communicate effectively with imaging departments and, minimally, enable cursory review of images.
- Extensive resources are available for neurologists to develop more detailed skills and expand their scope of contribution to the growing field of neuroimaging.

INTRODUCTION

MRI is central to neurologic diagnosis and treatment planning, with a rich history of innovations drawing on knowledge and insights from clinical neuroscience experts.[1–3] Recent advances in physiologic imaging, quantitative methods, informatics, artificial intelligence, and scan-time reduction are yielding more information with which to make early clinical diagnoses, but also resulting in greater complexity and the need for strong multidisciplinary communication among subspecialty professionals.

At least a rudimentary technical literacy of MRI is important for all clinicians who regularly refer patients for MRI. Although there are only a few procedure codes to consider when ordering an MRI, there should be an appreciation for the clinical detail required to select from the many MRI scanning protocols, sequences, and parameters that should be tailored precisely to answer the clinical question for that individual patient.[4] Furthermore, knowledge of fundamentals enables the ordering provider to ask about the availability of special techniques that may improve conspicuity of suspected

Disclosure Statement: N.K. Pinter and J.V. Fritz are consultants for Philips Healthcare.
[a] Dent Neurologic Institute, 3980A Sheridan Drive, Suite 101, Amherst, NY 14226, USA; [b] Department of Neurosurgery, State University of New York at Buffalo, Buffalo, NY, USA; [c] Dent Neurologic Institute, 3980 Sheridan Drive, Suite 501, Amherst, NY 14226, USA; [d] NeuroNetPro, Amherst, NY, USA
* Corresponding author. 3980 Sheridan Drive, Suite 501, Amherst, NY 14226.
E-mail address: jfritz@dentinstitute.com

Neurol Clin 38 (2020) 1–35
https://doi.org/10.1016/j.ncl.2019.08.002
neurologic.theclinics.com

pathologic condition, set expectations for the patient experience, and take advantage of readily available images to enhance shared decision making with patients. Ultimately, understanding the language of MRI permits a more successful collaboration between patient care and diagnostic imaging professionals.

The purpose of this article is to provide an overview of currently available MRI capabilities, and those in the process of becoming mainstream, to help the practicing clinician achieve these goals. A complete didactic is outside of the scope possible within this article, so the reader is advised to consult readily available papers, books, videos, and illustrations for additional detail on MRI techniques[5–9]; safety considerations related to contrast use, implanted devices or cosmetics[10–13]; and appropriate utilization guidelines used by payers and regulatory agencies.[14–16]

FUNDAMENTALS AND APPLICATIONS OF COMMON MRI SEQUENCES

An MRI imaging study comprises multiple series, each representing unique views tailored to the referring indications. Acquisition techniques are often referred to as sequences, a term derived from the sequential process of generating, receiving, and reconstructing signals from protons in tissue. A virtually unlimited number of permutations of technical parameters are available, leading to the versatility and complexity of MRI.

The primary goal in manipulating sequence parameters is to optimize contrast and anatomic views that improve lesion conspicuity. The timing parameters repetition time (TR), echo time (TE), and inversion time (TI) control tissue contrast; flip angle can reduce imaging time or offer an additional way to control the so called T1 weighting; matrix size, slice thickness, field of view, slice orientation, and whether the acquisition is 2-dimensional (2D; slice by slice) or 3-dimensional (3D; contiguous volume imaging) determine resolution and, therefore, detectability of small structures or lesions. Use of a gadolinium-based contrast agent (GBCA) reduces T1 and T2 relaxation time constants for affected tissue, thereby increasing pixel intensity of T1-weighted images, and reducing the intensity in T2-weighted images. T1-weighted images are generally performed before and after GBCA. The interconnectedness of its many parameters adds to the complexity of MRI, in which acquisition strategies constantly trade signal-to-noise ratio, resolution, scan time, and artifact mitigation.

A glossary of some of the more frequently used parameter terminology is presented in **Table 1**. **Table 2** summarizes sequences typically used for brain and spine imaging. **Table 3** lists some common artifacts.[17]

Basic Structural Scans

T1-weighted and T2-weighted sequences form the anchor for structural MRI using variations of Spin Echo (SE) or Field Echo (FE) sequences. Both SE and FE, as well as their accelerated versions Fast Spin Echo (FSE) and Fast Field Echo (FFE) rely on precise timing of excitations (TR) and readout (TE). An additional parameter called the Flip Angle (FA) can be varied to control the orientation of tissue magnetization, allowing trade-off between maximum signal, shorter scan time and more contrast control. **Fig. 1** illustrates the change in tissue contrast as TR and TE parameters are varied to control the degree of T1, T2, and proton density (PD) weighting. In general, T2 and T1 weightings produce reversed contrast between fat, white matter, gray matter, and cerebrospinal fluid (CSF) (dark to bright in T2 weighting, bright to dark in T1 weighting). Anomalies to this contrast ordering can occur with certain sequences. For example, T2-weighted fast spin echo (FSE) images may exhibit brighter than expected fat signal owing to the complex interaction of the many refocusing pulses with the tissue. In T1-weighted images, the typically bright fat signal may be intentionally suppressed

Table 1
Basic terminology

Term	Definition
Larmor Frequency	Natural precessional frequency of a proton that permits detection and localization of protons in tissues. Proportional to the magnetic field determined by the Bo (B zero, main static field of an MRI, eg, 1.5 T or 3 T), plus any temporarily applied gradient fields used for spatial encoding, plus any tissue effects that change the local field around the proton (eg, chemical structure or susceptibility)
RF pulse or RF excitation	Radiofrequency pulse, also known as the B1 field, tuned to the Larmor frequency that is used to excite the net magnetization of protons toward a perpendicular (measurable) orientation to the Bo field
Echo	Data that are obtained after RF excitation and represent a single "view." Multiple echoes or views are needed to reconstruct an image, similar to multiple projections obtained in CT
Receiver coil	The antenna that is applied to the patient anatomy being scanned. Receiver arrays consist of multiple coil elements to improve signal-to-noise ratio and, together with parallel imaging, speed up scans
TR	Repetition time, or the time between RF pulses that allows for tissues to realign with the magnetic field. Selected to determine T1 weighting. Also a primary determinant of scan time.
TE	Echo time. Time from excitation to echo readout. Selected to control T2 contrast
T1	A tissue property that represents the rate of recovery for excited tissue to realign with the main magnetic field
T2	A tissue property that represents the rate of dephasing (signal loss) in the transverse plane after excitation
T2*	Field echo version of T2, but also accounts for signal lost by not using a refocusing pulse (ie, T2* includes susceptibility effect)
Phase-encode (PE) direction	One of the 2 directions in an image. Specifies the direction in which the phase of the proton signal is used to decode position. The number of phase-encode steps, together with the field of view in the PE direction, determines resolution, is a primary determinant in scan time, and is the direction in which motion and wrap artifacts propagate
Frequency-encoding (FE) direction	A user-defined parameter that specifies the direction in which the magnetic field is changed to encode proton location by its Larmor frequency. Represents one of the 2 directions in an image, and is the direction in which chemical shift artifacts propagate
TI	Inversion time is the time delay parameter in an inversion recovery sequence. It is used to time the point at which certain tissue is nulled based on its T1 before initiating an imaging sequence, or to create a greater contrast in T1-weighted images. A short TI is used in STIR to null fat; a long TI is used in FLAIR to null CSF; and a midrange TI is used to stretch T1 contrast, for example, in high-resolution T1-weighted hippocampal imaging
Matrix	Specifies the in-plane resolution, or number of pixels that cover the field of view in the PE and FE directions (eg, 256 $\times$ 192). The matrix size in the PE direction determines the number of views required, and hence is a major determinant in scan time

(*continued on next page*)

Table 1
(*continued*)

Term	Definition
Field of view	The spatial extent of the imaging volume in the PE and FE directions (eg, 25 cm × 25 cm)
Slice thickness	Determines the voxel dimension in the slice direction
Pixel and voxel resolution	The area of the picture element in an image, or the volume of a voxel (pixel area times slice thickness). Higher resolution means smaller voxels and therefore less signal (fewer protons per voxel), but improved detail (less partial volume averaging)
Bandwidth	Specifies the range of precessional frequencies used for Frequency Encoding. Equates to how quickly a readout signal is acquired. Choosing a high bandwidth is advantageous in speed and reducing chemical shift artifact, but disadvantageous because of a decrease in signal-to-noise ratio
Echo train length (ETL)	The ETL specifies the number of FSE or FFE echoes during a single excitation period, reducing scan time proportionally
Parallel imaging, SENSE factor	Uses sensitivity profiles from individual elements of array coils to reduce scan time

Table 2
Common sequences used for brain and spine imaging

Spin echo (SE) and fast spin echo (FSE)	Routine structural imaging. Fast spin echo (also known as turbo spin echo) obtains multiple views (echo train) within a single repetition to proportionally reduce imaging time. • Proton density weighting (long TR, short TE) • T1 weighting (short TR. short TE) • T2 weighting (long TR, long TE)
Field echo (FE) and fast field echo (FFE)	Same as SE and FSE (TSE) except for eliminating a "refocusing" pulse to correct for loss of signal owing to magnetic field inhomogeneity. • Creates T2*-weighted images that enhance tissue susceptibility effects (eg, blood products) • Increases acquisition speed using shorter TR and lower flip angle, useful in 3D imaging
Inversion recovery	Manipulates T1 tissue contrast with an inversion pulse "TI" seconds before a conventional imaging sequence • Medium TI = greater T1 tissue contrast (phase-sensitive IR = PSIR) • Short TI or short tau IR = STIR for fat suppression and high lesion conspicuity • Fluid-attenuated IR = FLAIR for CSF suppression
Chemical shift–based fat-suppression methods	Different magnetic properties of fat and water cause their frequencies to differ, allowing for manipulation of fat and water signals. • Chemical shift or fat sat uses a prepulse tuned to the resonant frequency of fat • Out-of-phase FE imaging, water-fat separation, and Dixon methods use field echo sequences and specific TEs tuned to the different fat and water frequencies to add or subtract water and fat signals
Diffusion-weighted imaging	Relatively restricted movement of fluids causes bright signal. • Apparent diffusion coefficient (ADC) image provides quantitative value for rate of diffusion (bright DWI owing to restricted diffusion will be dark on ADC because the diffusion is low) • Diffusion tensor images map diffusion boundaries, such as along white matter tracts

(*continued on next page*)

Table 2
(*continued*)

Perfusion-weighted imaging (PWI)	• Dynamic susceptibility contrast (DSC) collects T2* images while GBCA contrast perfuses tissue. Dynamic contrast enhancement (DCE) uses dynamic T1 images. Typically calculate CBF, CBV, MTT, and/or TTP maps from pixel-by-pixel dynamic changes • Arterial spin labeling is a noncontrast perfusion technique using MRI pulses to mimic a GBCA bolus
Susceptibility-weighted imaging	A T2* acquisition with special postprocessing to enhance and quantify susceptibility effects. Generally used to accentuate conspicuity of, and differentiate, blood products and calcification
Driven Equilibrium or Fast Recovery FSE (DRIVE, FRFSE, RESTORE)	Additional RF pulse to speed T1 recovery. Improves brightness of long T1 tissue such as CSF. Typically used to create high-contrast, high-resolution T2-weighted images such as cranial nerve imaging
Magnetic resonance angiography (MRA)	Differentiates blood vessels from surrounding static tissue using sequences sensitive to flow. • Time-of-flight MRA uses a very short TR to create an excessively T1-weighted image (little signal). Inflowing blood that does not experience the short TR is relatively bright. • Phase-contrast MRA quantifies blood flow using special sequences sensitive to user-defined ranges of flow velocities, and is typically used for slow/venous imaging • Contrast-enhanced MRA uses very fast, heavily weighted T1 sequences timed to the injection of a contrast agent. Used for speed, a more accurate representation of vessel lumen, and dynamic visualization of flow
Whole-body imaging	Stitches together and creates projections of fat-suppressed STIR or DWI images that are sensitive to either diffusion restriction (hypercellularity) or long T2/short T1 pathology. Used as an oncology screen
Functional MRI (fMRI)	Uses Blood Oxygen Level Dependent (BOLD) technique to identify areas of the brain that correlate oxygenation-related signal changes and neural activity. The paradigm-driven method uses a dynamic acquisition during timed patient activities, and correlates signal changes to activity to determine areas of activation. Newer "resting state" functional imaging (rs-fMRI) correlates naturally occurring oxygenation changes across brain regions to identify functional connectivity. fMRI can be used with DTI to identify eloquent tissue and fiber tract connections as part of presurgical planning
Magnetic resonance spectroscopy	Identifies relative levels of metabolites such as lactate, NAA, creatine, choline, and myoinositol. Low NAA implies cell death, high choline implies hyperactive metabolism (tumor), myoinositol is associated with dementia. Image maps typically display colorized metabolite ratios

Table 3
Common MRI artifacts

Artifact	Description and Comments
Echo train blurring	Blurring in sequences with short TE and a long echo train. Caused by T2 signal loss while collecting multiple echoes
Wrap, aliasing	Anatomy from one edge of the field of view in the PE direction is misplaced to the opposite side of the field of view. When using parallel imaging to shorten scan time, which effectively stitches together smaller fields of view, the artifact can appear toward the middle of the image

(*continued on next page*)

Table 3
(*continued*)

Artifact	Description and Comments
Susceptibility	Signal loss and distortion associated with interfaces between tissues and objects with differing magnetic field properties, such as bone, air, metal, and soft tissue. Also the basis for susceptibility-weighted imaging of blood products
Chemical shift	Misplacement of fat signal along the FE direction, causing a bright/dark band at edge of fat-containing tissue
Pulsation and ghosting	Motion, including variable blood flow, creates replication "ghosting" along the phase-encode direction
MRA TOF artifacts: turbulent flow and venetian blind artifacts	Blood flow turbulence causes dephasing and exaggeration of stenosis; in multi-slab 3D TOF MRA, boundaries between slabs may exhibit abrupt signal changes
Nonuniform fat suppression	Caused by magnetic field distortion from susceptibility effects, equipment malfunction, or at the boundaries of the useable field of view for a given scanner
STIR suppression of gadolinium enhancement	Suppression of GBCA enhancement because of inappropriate use of STIR for fat suppression in postcontrast study
Gibbs/edge ringing	Replication of sharp boundaries when image resolution in PE direction is too low in a high-contrast area of an image, such as the CSF-cord interface in T2-weighted spine imaging

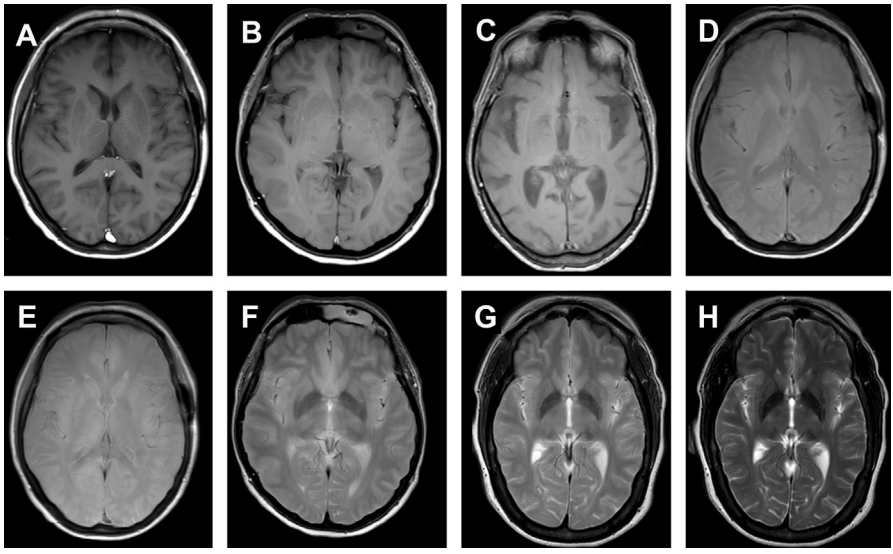

Fig. 1. Effect of sequence parameters on image contrast. In (*A*) through (*D*), TE is fixed at 10 ms while TR is set at 400 ms, 1000 ms, 1800 ms, and 3000 ms, respectively. This shows white matter signal decreasing and gray matter and CSF signal increasing as image appearance shifts from typical T1-weighted contrast (*A*) to typical proton density contrast (*D*). In images (*E*) to (*H*), TR is fixed at 3000 ms while TE is set at 10 ms, 70 ms, 90 ms, and 150 ms. The signal of white matter and deep gray matter structures decreases while the signal of CSF remarkably increases as image appearance shifts from a proton density contrast (*E*) to typical T2-weighted contrast (*H*).

through the use of a "chemical saturation" technique; this may be done, for example, to differentiate fat from contrast agent enhancement, or to eliminate an artifact that can misrepresent the location of fatty tissue resulting from a phenomenon called chemical shift. Fig. 2 demonstrates that structural imaging can itself offer functional insights.

Acquisition of some sequences in different imaging planes is not only helpful in visualizing the anatomy but also provides a check against certain artifacts that propagate along specific directions (eg, pulsatile flow can "ghost" in the phase-encode direction). Axial, sagittal, coronal, or oblique orientations are generally standardized to anatomic landmarks to provide consistency in interpretation, and when comparing series within or between studies.

3D acquisitions are high signal-to-noise ratio, time-efficient scans that offer versatile tissue contrast. An important benefit of a 3D scan is the ability to separately optimize the acquisition orientation and the anatomic view by using postprocessing rather than individual acquisitions to generate multiplanar reformatted views (Fig. 3).

Long TE field echo imaging generates are known as T2*-weighted rather than T2-weighted images. They are more sensitive to signal changes from magnetic field disturbances, whether from equipment or tissue interaction. Although this sensitivity does produce vulnerability to artifacts, T2* sequences offer certain advantages, such as blood product visualization (eg, hemosiderin and calcification are dark).

The concept of susceptibility-weighted imaging to view blood products has long existed using this basic T2*-weighted field echo sequence. However, today the term susceptibility-weighted imaging (SWI) has evolved to represent a more sophisticated version of a long TE field echo sequence, using "phase data" normally ignored in classic magnitude reconstructions to enhance subtle areas of susceptibility changes.

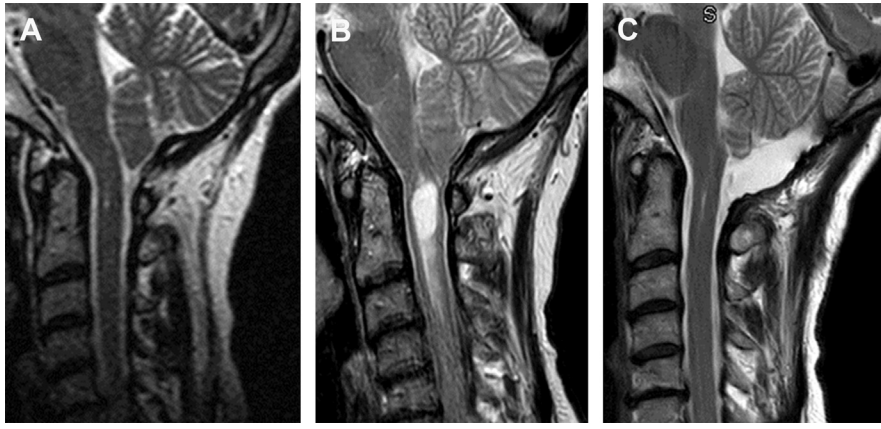

Fig. 2. Evolution of Chiari malformation and cervical syrinx in a 58-year-old patient. Sagittal T2-weighted sequence (*A*) shows cerebellar tonsils extending 3.5 mm below the foramen magnum and a subtle hyperintensity in the center of the spinal cord at C1 (A, *arrowhead*). Four years later (*B*), the tonsils extend 5 mm below the foramen magnum, consistent with Chiari I malformation; a large syrinx with surrounding edema developed at C1–C2 (*B*, *arrowheads* and *bracket*). (C) shows follow-up after decompressive surgery, with resolution of the syrinx. This case illustrates the interplay between structural changes and CSF flow dynamics in the evolution of syrinx and Chiari malformation, and calls attention to the role of functional diagnostics in the evaluation of abnormalities of the craniocervical junction.

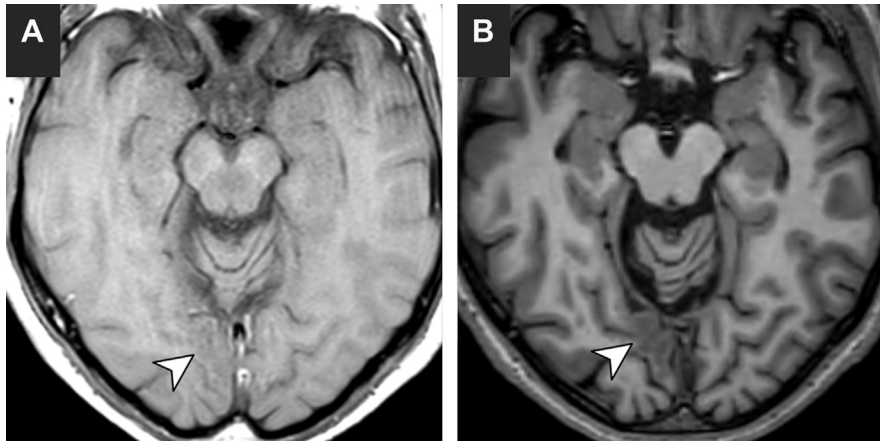

Fig. 3. Significance of 3D imaging in epilepsy diagnostics. (*A*) A 2D T1 scan with 4 mm slice thickness; (*B*) an axial reformat of a 3D T1 scan acquired in sagittal plane. Although the 2D acquisition has higher in-plane resolution (0.9 × 0.9 mm), the worse gray-white contrast and the flow artifact running in lateral (phase) direction from the straight sinus make the occipital focal cortical dysplasia (*arrowhead*) difficult to detect compared with the axial reformat that has slightly lower in-plane resolution (1 × 1 mm).

Standard variations include 2D, 3D, and thick slab "projection" views (minimum-intensity projections), along with display of "phase maps" that are used to differentiate blood products from calcifications. Compared with conventional T2* imaging, SWI is superior in venous imaging, amyloid angiopathy, trauma, and various causes of microbleeds (**Fig. 4**). Newer developments seek to quantify the degree of susceptibility and relate that value to oxygenation.[18]

3T magnetic resonance systems are often preferred over 1.5 T and lower field strengths for neuroimaging because of advantages in signal-to-noise ratio, higher-resolution scanning, and improved lesion conspicuity. However, 3T does require higher-power RF pulses, which increases the rate of heat buildup in a patient. Specific absorption rate (SAR) limitations are built into MRI systems to ensure patient safety, but can result in slower scans. For this reason, 3T MRI sequences have been adjusted to minimize the use of high-power pulses, such as greater use of use of 2D and 3D field echo sequences.

T2*-related distortion from metal or pulsatile flow tend to be greater, however, and 3T MRI further exacerbates these artifacts. In contrast, spin echo (SE) or turbo spin echo (TSE) sequences (T1, T2, or PD contrast) offer better signal-to-noise ratio and tend to self-correct for artifacts caused by tissue interactions with the magnetic field, and blood flow tends to create signal voids that minimize pulsatility artifacts while providing helpful views of major vessel lumens and aneurysms. In recent years, special sequence methodologies have been created to increase the speed of 3D SE sequences through longer echo trains and novel approaches to reduce the SAR effect of many refocusing pulses. 3D field echo sequences remain the norm for T1-weighted 3D acquisitions, although 3D TSE sequences are becoming more popular for long TE, T2-weighted imaging.

The following sections provide an overview of other structural and physiologic imaging techniques, selected to highlight certain practical aspects that the authors consider important based on their experience. The discussions are not intended to

Fig. 4. Severe amyloid angiopathy on SWI showing innumerable hemorrhages in cortical and subcortical localization in both hemispheres. There is a striking contrast between the appearance of the spared basal ganglia and thalami and of the heavily affected peripheral parenchyma. Larger hemorrhagic foci are seen in the left frontal and temporal lobes (*arrows*). Areas of superficial siderosis are also noted in the posterior parietal lobes (*arrowheads*), resulting from prior subarachnoid hemorrhage of superficial lesions.

be comprehensive, but rather to provide clinically useful takeaway points and ignite interest in current and future methods.

Inversion Recovery and Fluid-Attenuated Inversion Recovery

Fluid-attenuated inversion recovery (FLAIR), or more specifically T2 FLAIR, has become an essential part of brain evaluation because the suppression of CSF signal produces excellent contrast between lesions and white matter. With a few exceptions, lacunar infarcts in the basal ganglia being one, it is superior to T2-weighted images in lesion visualization.

Improving contrast by eliminating CSF signal has always been important for clinical scanning and until as recently as the mid 2000s, proton density (PD) was the primary technique used for this purpose because of its relative "dark CSF" appearance (see **Fig. 1**). Starting in the mid 2000's, FLAIR has become the primary sequence for detection and monitoring of demyelinating lesions.[19,20] Advances in technology for 3D FSE techniques have resulted in the ability to perform time-efficient 3D FLAIR, which offers superior signal, reduced artifacts, and improved resolution compared to 2D scans.- **Figs. 5** and **6** illustrate advantages of 3D FLAIR.

FLAIR is a variation of the inversion recovery (IR) technique, which manipulates tissue contrast based on T1 characteristics; short tau IR (STIR) suppresses T1 fat, dual IR

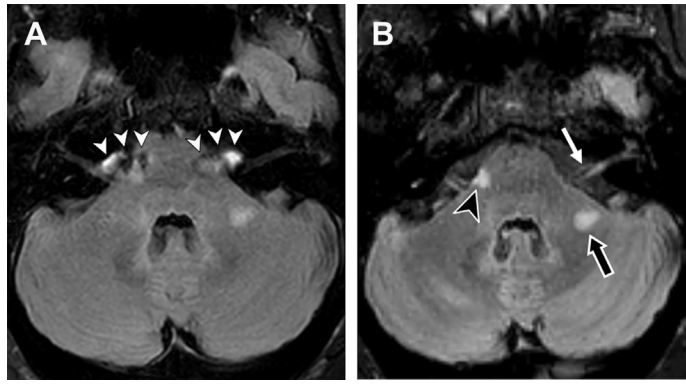

Fig. 5. On 2D FLAIR (*A*), prominent CSF pulsation artifacts are seen in the cerebellopontine angles (*white arrowheads*), obscuring a demyelinating lesion in the right lateral aspect of the pons, which becomes visible on 3D FLAIR (*B*, *black arrowhead*). With 3D acquisition the fluid attenuation in cerebellopontine cisterns is homogeneous, allowing sharp visualization of not only the pons, but the 7th and 8th cranial nerves as well (*B*, *white arrow*). A second lesion is seen in the middle cerebellar peduncle on the right, which is also more conspicuous on 3D (*B*, *black arrow*).

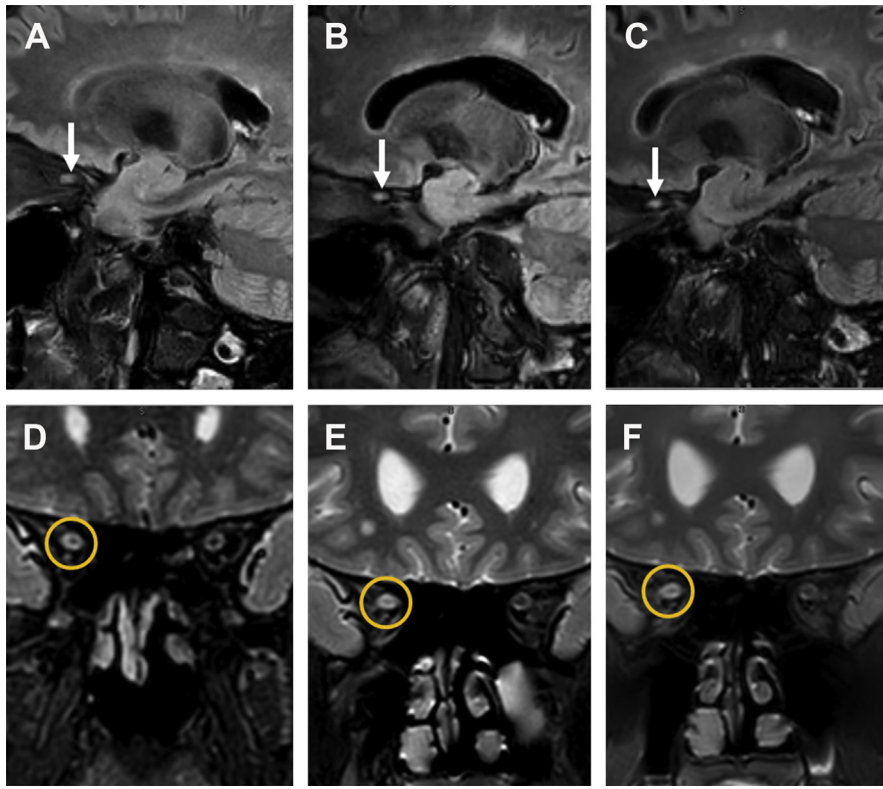

Fig. 6. Serial imaging of optic neuritis. On the sagittal 3D FLAIR, the right optic nerve shows a short, segmental hyperintensity that stands out against the background (*arrow* in *A*–*C*). On coronal fat-suppressed T2-weighted images, the affected nerve is depicted with smaller caliber and higher signal intensity compared with the normal left optic nerve (*circled area* in *D*–*F*). During the course of the longitudinal follow-up, the abnormality shows up consistently on both sequences and is more conspicuous on the 3D FLAIR. This draws attention to the broad utility of 3D FLAIR in imaging of multiple sclerosis.

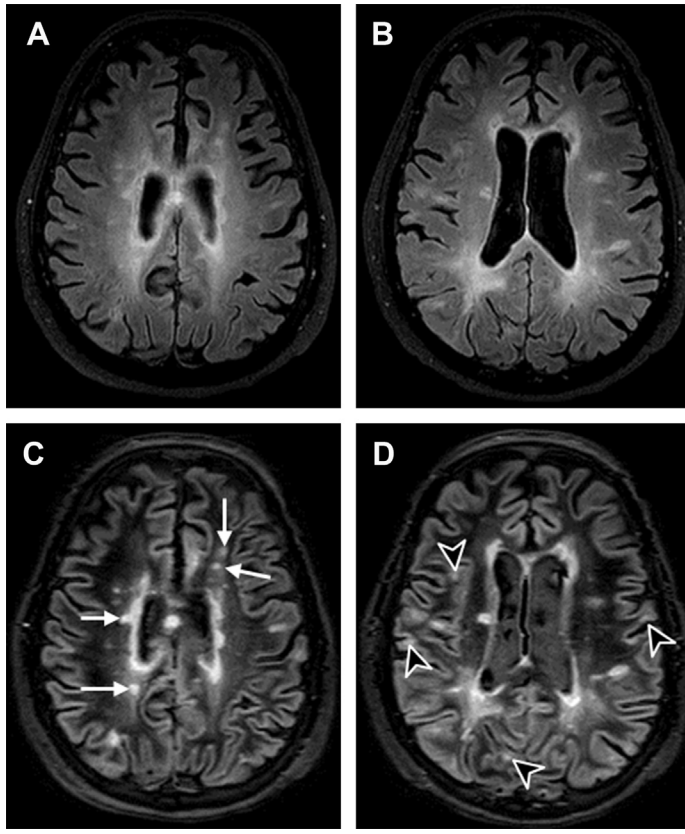

Fig. 7. Demyelinating lesions are shown on 3D FLAIR (*top row*) and 3D double inversion recovery (DIR, bottom row) in multiple sclerosis.(*A–C*) and (*B–D*) image pairs show the same slices. Increased lesion contrast is seen on the DIR images, which allows for an improved differentiation of deep white matter lesions (*white arrows* in *C*) as well as juxtacortical and cortical lesions (*arrowheads* in *D*).

uses multiple inversion pulses to suppress both CSF and white matter (Fig. 7), and phase-sensitive IR (PSIR) uses a midrange inversion time (TI) to stretch the T1 contrast of tissues.

Diffusion-Weighted Imaging

The diffusion-weighted sequence has high sensitivity to very slow flow, causing signal loss from normal extracellular fluid diffusion, and relatively bright signal in areas of abnormally restricted fluid motion. The flow sensitivity is controlled by a parameter known as the "b-value". At a b-value of zero, the image is essentially a conventional T2*-weighted image. At a b-value of 1000, normal tissue diffusion causes significant loss of signal. The b1000 image is typically referred to as the diffusion-weighted image. The b0 and b1000 images can be mathematically combined to calculate an apparent diffusion coefficient (ADC) image, which provides a numerical value for each pixel that equates to tissue diffusion. The purpose of an ADC image is to isolate the diffusion effect from other T2* effects that can cause the diffusion-weighted image to be bright (this is known as T2 shine-through). Bright pixels on a diffusion-weighted

image should correspond to pixels with low diffusion coefficient values (dark pixels) on ADC, as long as the bright diffusion-weighted area is related to diffusion restriction and not T2 shine-through (**Fig. 8**). It is crucial that ADC is the "reality check" for diffusion-weighted imaging (DWI), meaning that **DWI cannot be reliably interpreted without the ADC map**.

DWI is very useful in differential diagnostics. It provides relevant information quickly and is generally easy to interpret. Abnormalities that will typically appear with high signal intensity on the DWI b1000 image and with corresponding low signal on ADC ("DWI positive") are associated with restriction in normal motion of the water molecules. Examples include: cytotoxic edema in acute infarcts when the water moves from the large extracellular space (where it is relatively free to move along white matter tracts) into the smaller intracellular space where its motion is confined in every direction; pus (ie, thick cellular debris) in an abscess where there is no real water diffusion; hypercellularity in some tumors with the most well-known example being primary central nervous system lymphoma; accumulation of material such as cholesterol and keratinous content in an epidermoid blood or even acute venous thrombosis; or again, cytotoxic edema in acute demyelinating plaques.[21,22] Other scenarios when DWI can be positive (ie, it shows restricted diffusion compared with normal tissue) include metabolic encephalopathies and degenerative disorders, such as Creutzfeld-Jakob disease, hypoglycemia, carbon-monoxide (CO) poisoning, hepatic encephalopathy, or osmotic demyelination syndrome, to name only a few.[23]

The opposite, increased diffusion, appears dark *or* bright on b1000 and *always* bright on ADC. Any tissue that has a buildup of freely moving water content will show high signal on ADC relative to normal parenchyma: from arachnoid cysts to liquefaction in chronic infarcts to cystic components in tumors to vasogenic edema (see **Fig. 8**).

Diffusion tensor imaging (DTI) is a reconstruction of directional diffusivity from multiple DWI sequences that probe proton mobility in several directions. Images representing average diffusivity and fractional anisotropy (FA) maps are created to characterize the magnitude of diffusion, its prominent direction, and directional distribution (tensor) within each voxel. The pixel FA value quantifies the ellipsoidal nature of diffusion, ranging from 0 for spherical (isotropic) diffusion in which there are no boundaries, to 1 for voxels that exhibit linear diffusion, such as along intact white matter tracts. Cautious use of functional MRI (fMRI) and DTI can provide a helpful visualization of eloquent tissue and related interconnections for presurgical planning or assessing the mass effect of a tumor (**Figs. 9** and **10**). Although the terms "pathways" and "tracts" are used, these color-coded images are representations of FA in the image voxels, which are large compared with real fiber size and thus are only a rough estimate of the real pathways. Quantitative FA maps may have value in determining the degree of white matter injury.[24–26]

DWI typically uses echo planar imaging (EPI), a very fast "single-shot" (1 minute) version of a field echo sequence. In general, EPI methods are very sensitive to susceptibility-related geometric distortion and signal loss at bone, air, tissue and metal interfaces (**Fig. 11**). Thus, the brain typically has a distorted shape on DWI images compared with other structural scans, with areas of artifactual high signal ("false positive") and signal loss along the frontal skull, the temporal bone, in the posterior fossa, and along any metal implants. This will make it difficult (and often impossible) to detect abnormalities in the brainstem, in the vicinity of surgical clips, in the presence of orthodontic appliances, adjacent to ventriculoperitoneal shunts or deep brain stimulation electrodes, and even in uncomplicated cases in the basal areas of the temporal lobes and in the orbital frontal cortex. EPI-based DWI can be replaced by TSE

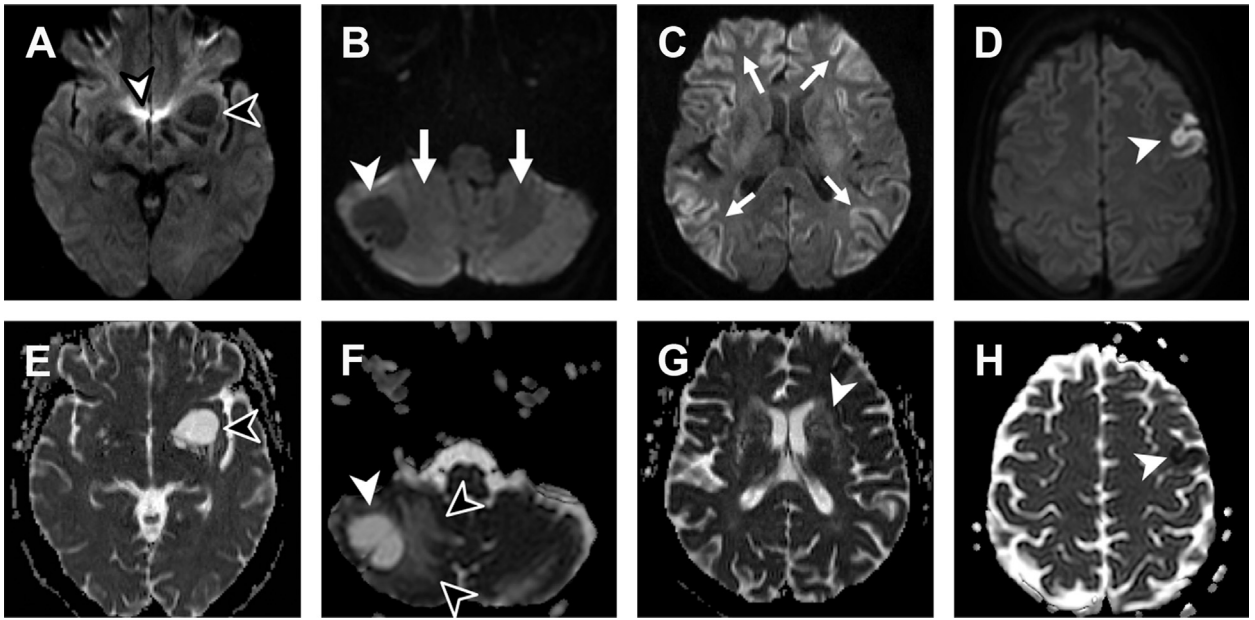

Fig. 8. DWI b1000 (top row) and corresponding ADC images (bottom row) from 4 cases. (*A–E*) Giant Virchow-Robin space in the area of the left basal ganglia (*black arrowhead*). The signal of the abnormality follows CSF on every sequence. Susceptibility artifact is creating high signal and distortion on DWI (*white arrowhead*). (*B-F*) Cystic tumor in the right cerebellar hemisphere (*white arrowheads*). Its appearance is similar to that of the enlarged perivascular space in (*A–E*); however, there is vasogenic edema in the parenchyma, which is prominent on ADC (*F, black arrowheads*). On DWI the edema appears as only a mild increase of white matter signal compared with the normal left side (*B*, *white arrows*) owing to T2 shine-through. (*C–G*) Diffuse cortical diffusion restriction is seen on the DWI image in both frontal lobes, parietal lobes, and insula, typical for Creutzfeld-Jakob disease (*arrows*). ADC is less demonstrative of these findings. In the basal ganglia increased diffusion is seen on ADC, owing to the high number of enlarged perivascular space (L'etat crible, *white arrowhead* in *G*). (*D and H*) An acute cortical infarct with diffusion restriction as demonstrated by the high DWI signal and corresponding marked ADC hypointensity.

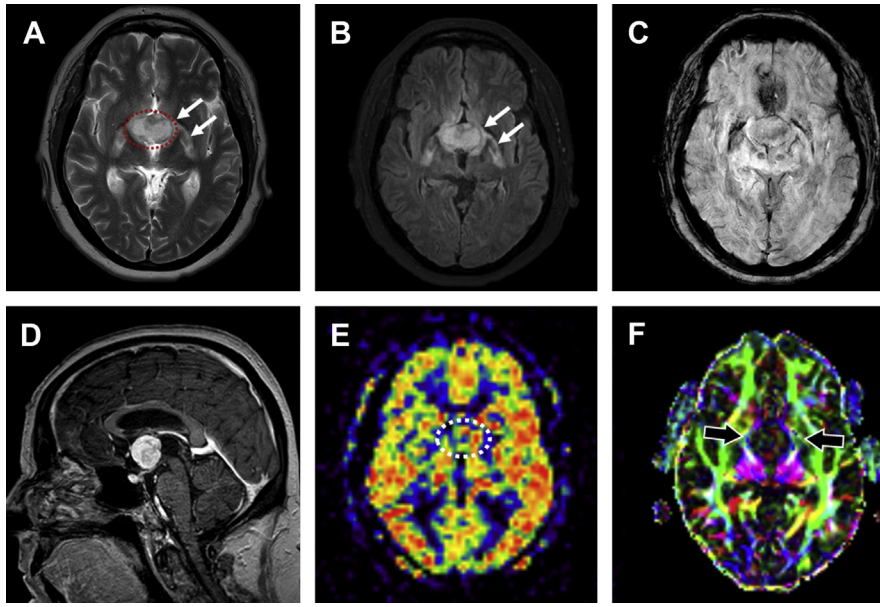

Fig. 9. Multiparametric imaging of a chordoid glioma. The tumor has hyperintense signal on T2-weighted image (*A*, *red dashed circle*) and FLAIR (*B*). No blood products or calcification are found on SWI (*C*), and homogeneous contrast enhancement is seen on 3D T1 (*D*). The 2D pCASL scan is unremarkable, without evident increased perfusion (*E*). The overall morphology and the perfusion findings are consistent with a benign tumor. Although bilateral minimal edema is seen in the basal ganglia and diencephalon (*arrows* in *A*, *B*) the adjacent white matter tracts are displaced and no true destruction is found on the fractional anisotropy map (*F*, *arrows*).

methods to mitigate artifacts, but results in a substantially longer scan (5–6 minutes). Decisions on applicability of DWI or which variation to use depend on relevant clinical information.

Magnetic Resonance Angiography: Time-of-Flight and Contrast-Enhanced Magnetic Resonance Angiography

There are 3 distinct methods for creating angiographic images in MRI: time-of-flight (TOF) magnetic resonance angiography (MRA), contrast-enhanced (CE) MRA, and phase-contrast (PC) MRA.

TOF MRA relies on bright signal from blood that enters an imaging volume that has low signal because of short TR saturation. There are 2D and 3D variations. 3D TOF MRA results in greater signal and resolution and is the usual scan for intracranial arterial imaging. 2D TOF is better for slow, venous flow, which tends to blend in with static background tissue in 3D volumes. However, 2D TOF has relatively poorer signal-to-noise ratio and resolution and is less commonly used than PC MRA or CE MRA.

Vessel lumen size can be estimated from the cross-section of the bright pixels, but only with caution because TOF works best with laminar flow and the flowing blood loses signal when turbulent flow occurs—one typical example being the carotid syphon. In general, TOF has a high negative predictive value but a low positive predictive value. For this reason it is widely accepted for aneurysm imaging, but less so for

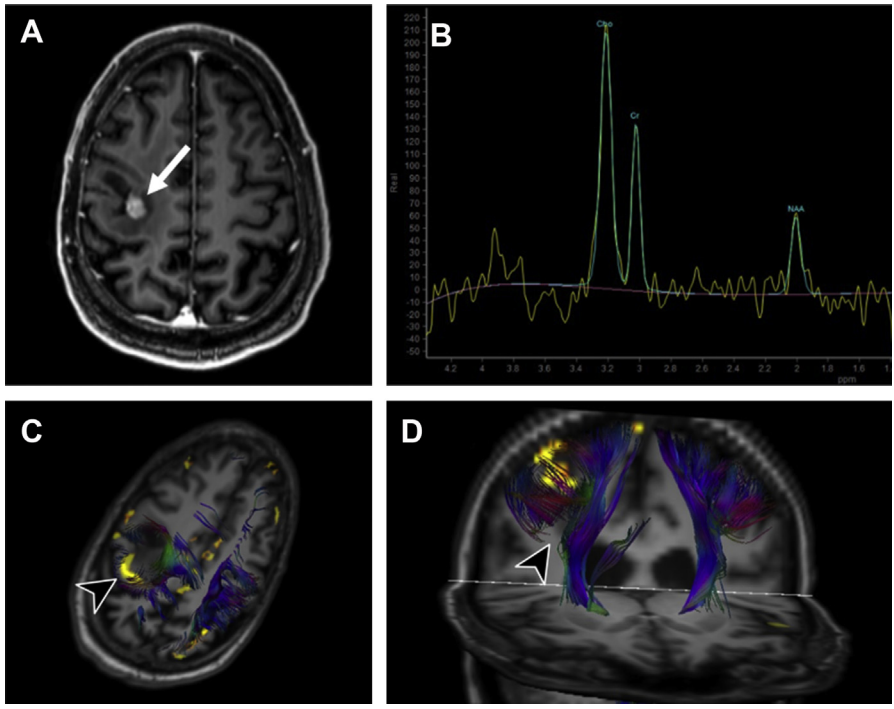

Fig. 10. Presurgical evaluation of an anaplastic astrocytoma shows a right posterior frontal mass with central contrast enhancement (*A*, *arrow*) and abnormal spectrum with elevated choline and decreased Cr and NAA in the same area (*B*). In (*C*) and (*D*) the fMRI motor activation map and tractography of the corticospinal tracts are shown, merged with the non-enhanced 3D T1 image. The most prominent activation during the left finger tapping paradigm is seen just posterior to the tumor, in the displaced and infiltrated precentral gyrus (*C*, *arrowhead*). The tractography shows fewer "tracts" on the right and abruption of the corticospinal pathways (*arrowhead* in *D*). The abnormal findings on DTI likely resulted from the combination of vasogenic edema and disruption of white matter microstructure owing to tumor infiltration.

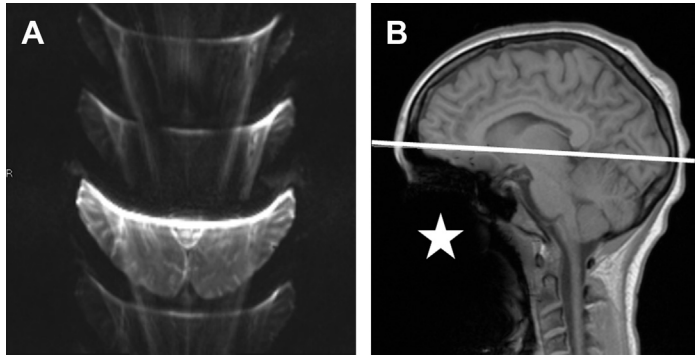

Fig. 11. Prominent susceptibility artifact is seen on DWI image (*A*), caused by orthodontic appliance in a young patient. Sagittal T1 (*B*) shows the angulation of the axial DWI (*white line*) and a large area of signal void overlying the oral cavity and facial tissue (*asterisk*), also caused by susceptibility for magnetic field changes. The DWI artifact might be reduced if the slices are aligned more parallel with the frontal skull base.

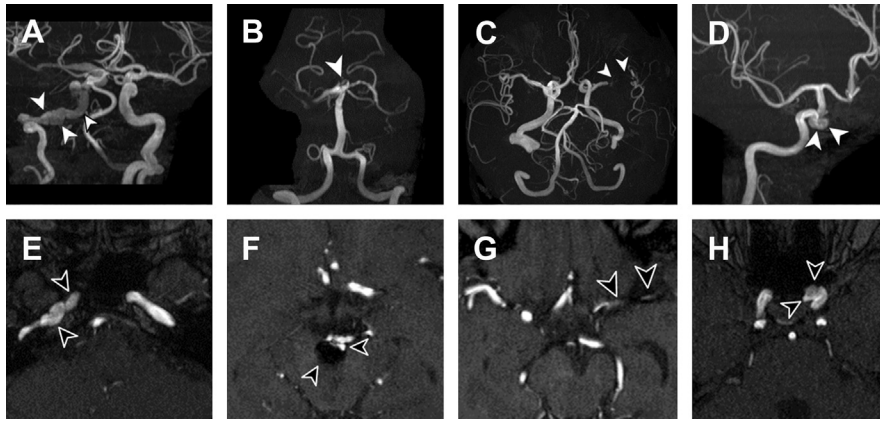

Fig. 12. 3D maximum-intensity projection images and corresponding to time-of-flight (TOF) MRA source images from 4 cases. (*A–E*) Fibromuscular dysplasia of the right internal carotid artery. (*B–F*) Basilar tip aneurysm following coiling. The arrowheads in (*F*) point out the residual flow in the basilar tip and the large susceptibility artifact caused by the coils. (*C–G*) Stent in the left middle cerebral artery (MCA) after acute stroke. No flow signal is seen in the MCA, which is again caused by susceptibility artifact and not the complete lack of flow, evident by the intact signal in the peripheral MCA branches. For stent evaluation, therefore, CT angiography is recommended. (*D–H*) Saccular aneurysm on the intracavernous segment of the left internal carotid artery (ICA). This location is more frequent than one would expect.

imaging of intracranial stenosis. It overestimates the degree of stenosis, and CT angiography is more reliable in that regard. The TOF scan consists of about 150 to 160 images (source images), which are then used to create 3D reconstructions (a virtual cast of vasculature) with a method called maximum-intensity projection (MIP). MIP images are routinely created for evaluation, but the final conclusion should never be made solely on MIP images because the reconstruction parameters are arbitrary and can (and almost always will) change the appearance of some vessels, potentially leading to false-negative or false-positive findings. The final decision should always be based on the source images (Fig. 12).

CE MRA uses fast 3D imaging after contrast agent injection to differentiate blood from static tissue. The technique requires proper timing between bolus injection and imaging, which can be more difficult for patients with vascular disease, and repeated CE MRAs in the same session are not recommended. An advantage of CE MRA is the ability to use cine views to visualize flow characteristics. CE MRA tends to be the preferred MRA technique for carotid imaging, as long as the patient is able to tolerate the contrast agent.

Imaging of Cranial Nerves: Driven Equilibrium, Constructive Interference in Steady State, and Other Useful Sequences

Heavily T2-weighted sequences that seek high contrast between CSF and parenchyma with a submillimeter resolution can result in very long scan times (many views, very long TR to allow full CSF signal recovery). Driven equilibrium techniques, such as DRIVE (driven equilibrium), RESTORE, or forced recovery FSE, help reduce scan time by using a somewhat shorter TR together with additional pulses to force longitudinal recovery. To further reduce scan time when the focus

is on high CSF contrast and not parenchymal detail, a very long echo train length can be used, which blurs short T2 tissue but leaves resolution intact for a long T2 CSF signal. Although the scan duration is still long (5–6 minutes) and should only be used with strong clinical justification, these high-resolution scans are excellent in visualizing small tissues bathed by CSF, such as cranial nerves. DRIVE is popular for vestibular nerve imaging to evaluate for potential vestibular schwannoma, and also useful in imaging of trigeminal nerve and other cranial nerves (CN3, CN6, CN9–12). **Fig. 13** demonstrates the use of DRIVE in the evaluation of neurovascular compression in trigeminal neuralgia, when coregistered with a TOF MRA.[27]

Another well-known sequence in this space is CISS (constructive interference in steady state),[28] which has a T1 component and thus can be used to assess abnormal contrast enhancement, and is helpful in inflammatory or cancerous processes involving cranial nerves or the Meckel cave. However, even without special scans the cranial nerves are often visible on a high-resolution 3D T1 (the CE scans can be

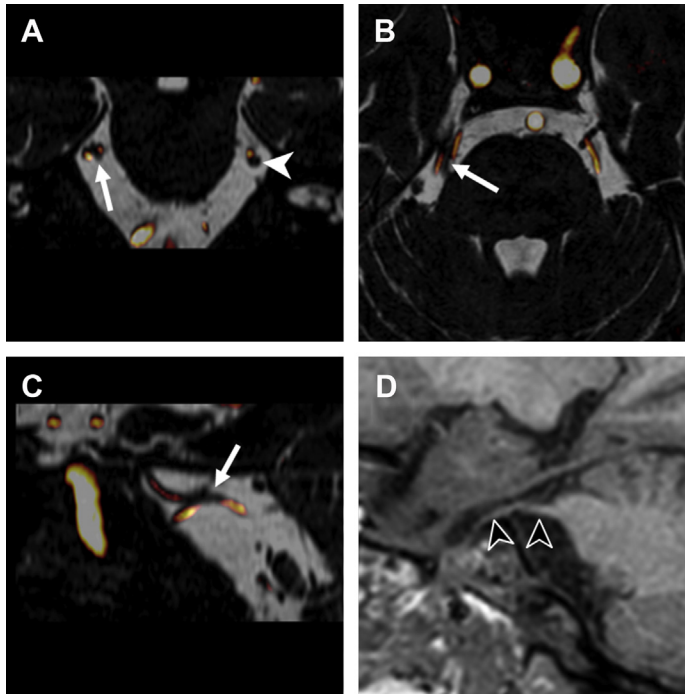

Fig. 13. Fusion of 3D DRIVE and TOF MRA images is shown in coronal, axial, and sagittal planes (*A–C*, respectively). The merging of the two image series is easily performed on a clinical postprocessing workstation. This visualization makes it easier to understand and interpret the relation between arteries and nerves and is useful in the evaluation of neurovascular conflict. In this patient, the trigeminal nerve on the right is compressed by the superior cerebellar artery and the anterior inferior cerebellar artery as highlighted by the arrow in (*A–C*). On the coronal image, the cross-section of the compressed nerve is elliptical in contrast to the rounded shape of the unaffected nerve on the left (*white arrowhead* in *A*). On the high-resolution sagittal 3D T1 (0.9 mm isotropic, *D*) the trigeminal nerve is clearly seen (*black arrowheads*); however, the small arteries are not visualized, thus the assessment of the neurovascular contact is not possible (compare *C* with *D*).

particularly satisfying for imaging the mandibular and maxillary nerves) or 3D FLAIR (can be surprisingly good for the abducens nerve). When a clinical question concerning a cranial nerve is left unanswered after a routine MRI, a second look on the image set is often good enough to find the answer and can spare the time, stress, and cost of an additional MRI examination- naturally, such additional investigation relies on a clear clinical question and good communication between the clinician and the radiologist.

Phase-Contrast Angiography

Phase-contrast angiography (PCA) is generally used for imaging of venous flow and is often referred to as magnetic resonance venography (MRV) in clinical practice. Its velocity sensitivity allows for visualization of the slower venous blood flow, making it a good alternative to contrast-enhanced (CE) computed tomography (CT). Flow sensitivity is defined by the parameter *velocity encoding* or "Venc," which specifies the expected velocity range. This property of PCA has two important practical implications: (1) if the Venc is too high, it will be difficult to differentiate variations of much slower normal venous flow representative of anatomic or physiologic variations; (2) if the Venc is too low, the intensities of higher velocities create variable intensity artifacts because their flow is misrepresented into the expected range (eg, if the Venc encodes velocities from 0 to 10 cm/s, an actual velocity of 16 cm/s "wraps around" and maps to 6 cm/s).

A typical case is the unilateral hypoplasia of the transverse sinus, when the sinus with the smaller caliber has slower venous flow that does not show up on PCA with a high Venc and mimics thrombosis. Concurrent hypoplasia of the internal jugular vein may also be present. This false positivity can be overcome easily by lowering the Venc to 5 to 10 cm/s whereby slower flow becomes visible; with this simple step one can both eliminate the possibility of a potentially life-threatening condition and spare further imaging tests. However, this lower Venc image becomes less clean as new flow-related artifacts appear. Although presaturation suppression of arterial blood helps to eliminate some artifact, the lower Venc is mostly used as an additional scan after the regular PCA scan, and only in dubious cases.

When there is a high likelihood of sinus thrombosis or occlusion of a small vein a 3D PCA must be done, as it creates a high-resolution image of the intracranial venous system. The 3D scans, however, take 5 to 6 minutes. Therefore, the 3D imaging should be done only in cases with high likelihood of thrombosis. Arteries are more prominent on 3D PCA, and proper interpretation requires experience.

Conversely, to quickly rule out a large sinus thrombosis when it is a less likely cause, such as in a patient with headaches, two fast, low-resolution 2D PCA sequences with 1 or 2 thick slices (20–40 mm, also called a "slab") and with low Venc can be applied, one in sagittal and another in axial plane, over the main venous sinuses. These 15- to 25-second scans have high clinical value, showing evident flow signal in the sinuses in healthy cases, allowing for a quick "rule-out" of large thrombosis.

An important source of false-positive results when using MRI to rule out sinus thrombosis is to misdiagnose arachnoid granulations as thrombus (**Fig. 14**). In most cases the morphology and signal characteristics makes the diagnosis evident, and with the proper amount of supervised training and experience this should be an error easy to avoid; however, this mistake still occurs in clinical routine. The importance of differentiating arachnoid granulations from thrombosis cannot be overstated because false-positive studies can result in unnecessary diagnostic tests and therapeutic interventions.

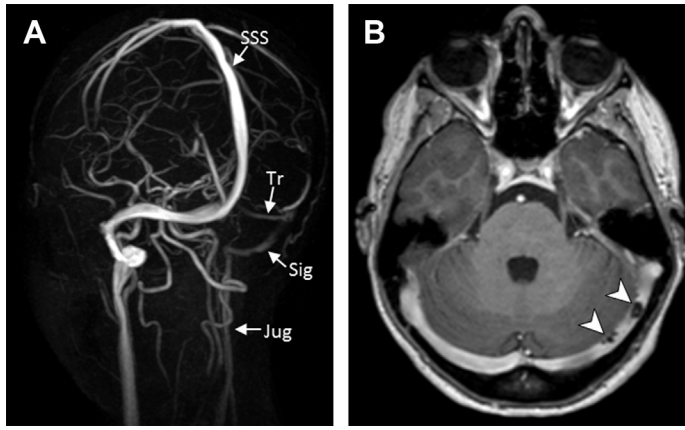

Fig. 14. MIP reconstruction of 3D PCA (*A*) shows low-intensity flow signal in the left transverse (Tr) and sigmoid (Sig) sinuses and in the left jugular vein (Jug). Normal flow is seen in the contralateral identical vessels and in the superior sagittal sinus (SSS). These findings are due to anatomic variation, most likely unilateral hypoplasia or slow flow. However, the contrast-enhanced T1-weighted (*B*) images show two well-defined, rounded filling defects in the transverse sinus (*arrowheads*). These are characteristic to arachnoid granulations, but in the presence of the PCA findings they may be mistaken for sinus thrombosis, although their presence is coincidental.

Of note, principles of PC MRA also apply to quantitative flow (Q-flow) imaging. Q-flow is often used in the diagnosis of normal pressure hydrocephalus, in which dynamic 2D or 3D dynamic acquisitions, gated to the cardiac cycle, measure and visualize CSF flow through the cerebral aqueduct.[29]

Fat-Suppression Techniques for Contrast-Enhanced Studies of the Spine

CE spine examinations should always be performed with fat suppression. Much can be gained and little will be lost. Without eliminating the signal from the adipose tissue, abnormal contrast enhancement can be completely missed, as it can be masked by the (equally high-intensity) signal of fat (**Fig. 15**). A widely used fat-suppression technique in spine is fat saturation ("fat sat", also known as chem sat), whereby a selective saturation pulse is applied at the beginning of the T1 pulse sequence to spoil the fat signal.[30] The end result will be a T1-weighted image minus the fat. This method can be sensitive to magnetic field inhomogeneities, but less so with the introduction of multitransmit magnetic resonance technology.[1]

Since CE T1 scans are done with fat saturation, should the same be done for precontrast scans? Ideally, yes: for good comparison it is preferred if both pregadolinium and postgadolinium scans are done with fat suppression. However, it is also generally important to have fat information; however, doing T1 scans both without and with fat sat in all relevant planes would add 5 to 15 minutes to the examination. Furthermore, it may be difficult to determine the relevant scan planes before adding gadolinium.

An alternative to conventional fat saturation and a good practical solution for this conflict is the Dixon method, which collects sufficient information in a single acquisition to decode multiple image representations: “fat,” “water,” “water plus fat,” and “water minus fat” images.[31] This sequence is robust in its ability to produce homogeneous images of these four distinct types. Its drawback is that it tends to be

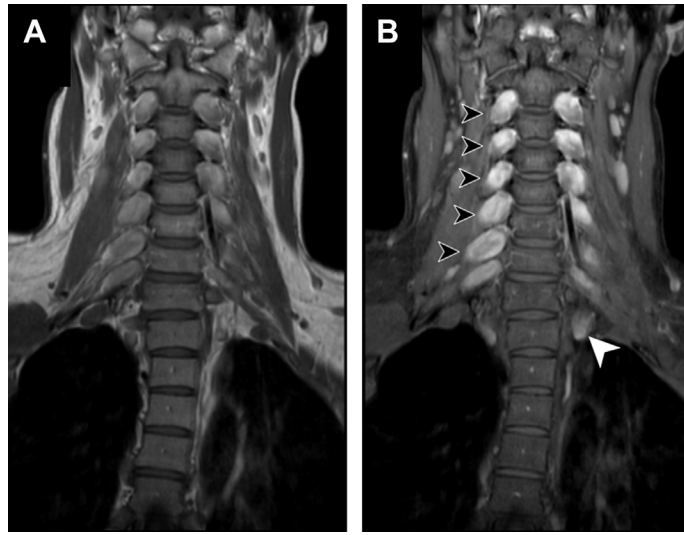

Fig. 15. Multiple cervical schwannomas are shown on contrast-enhanced T1 without fat suppression (*A*) and with fat suppression (*B*). The contrast-enhancing lesions are much more conspicuous in *B* (*black arrowheads*), demonstrating the importance of fat suppression in contrast-enhanced spine studies. The lesion at Th1–2 on the left is only visible in *B*, while completely obscured by fat signal in *A* (*white arrowhead*).

acquired at lower resolution than conventional T1 fat-saturated images owing to scan time.

As mentioned earlier, STIR is a popular fat suppression technique that is utilized widely in spine imaging to detect bone marrow edema. It is critical to note that STIR should never be used after GBCA injection, because the signal of the contrast agent will be nulled along with the fat resulting from its short T1 time (Fig. 16). This practically means that if one tries to create a contrast-*enhanced* STIR by administrating GBCA, inevitably a contrast-*reduced* image will be created.

Perfusion

The classic approach to measure relative tissue perfusion is dynamic susceptibility contrast (DSC) and to a lesser extent dynamic contrast enhancement (DCE), with applications in stroke, tumor, dementia, and multiple sclerosis.[32,33] In both methods, a contrast agent bolus is injected and a dynamic scan is obtained. As contrast reaches tissue, a T2* sequence undergoes susceptibility-related signal loss (DSC), or a T1-weighted sequence undergoes signal enhancement (DCE). The characteristics of the dynamic pixel-by-pixel flow pattern can be mathematically converted to cerebral blood volume (CBV), cerebral blood flow (CBF), mean transit time (MTT), and time to peak (TTP) maps and displayed as perfusion images (Fig. 17).

Arterial spin labeling (ASL) is a more repeatable alternative, since it does not require gadolinium injection. It replaces the exogenous GBCA agent with a simulated contrast bolus in the form of a separate MRI excitation (endogenous contrast) to blood vessels entering the imaging volume.[34] In clinical practice, ASL proves to be a heavily operator-dependent technique because of physiologic and anatomic variations, and therefore requires close attention and individual case-based quality

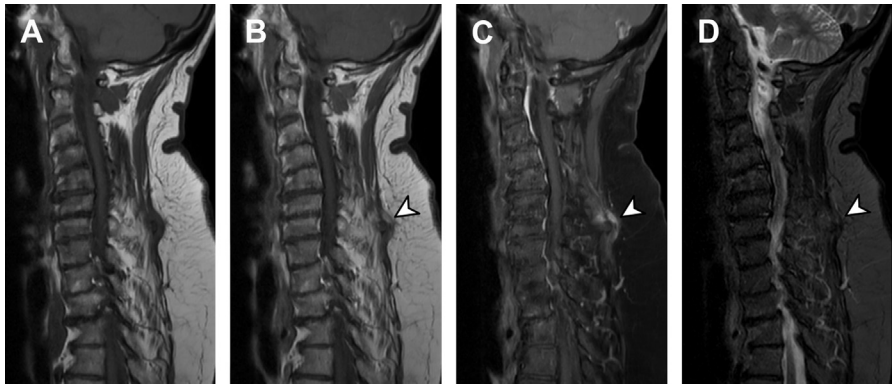

Fig. 16. Severe chronic degenerative disease of the cervical spine is seen on nonenhanced T1-weighted image (*A*). An area of abnormal contrast enhancement is noted in the soft tissue adjacent the C7 spinous process, indicating ongoing inflammatory process (*B–D*, *arrowhead*). This abnormality is difficult to distinguish on the regular contrast-enhanced T1-weighted image without fat suppression (*B*), while it is very conspicuous on contrast-enhanced T1 with fat saturation (*C*). However, on contrast-enhanced STIR (*D*), the lesion "disappears" owing to the suppression of the gadolinium signal along with fat signal, demonstrating why it is unwise to perform STIR following the administration of gadolinium-based contrast agent.

control.[35] This is most obvious in the elderly and in patients with cardiovascular or cerebrovascular disease, but occurs in younger and healthy individuals as well, resulting from variations of vascular anatomy. This naturally has consequences on the workflow, both in scanning and in interpretation. **Fig. 18** illustrates how normal anatomic variations can affect ASL results and may lead to the underestimation of cerebral perfusion. It also highlights the importance of planning the

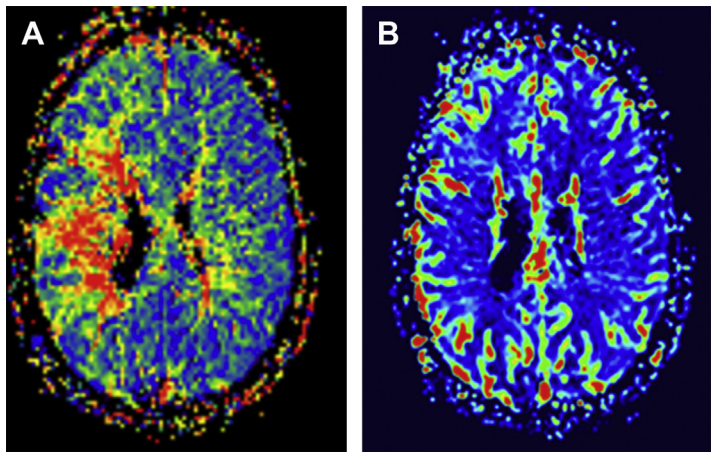

Fig. 17. Perfusion abnormalities in Moya-Moya disease on dynamic susceptibility contrast–based perfusion. Prominent delay is seen on the mean transit time map (*A*) in the right hemisphere, indicating that blood arrives via collaterals to this area. The cerebral blood volume map (*B*) however shows no regional rCBV deficit, suggesting that the collateral supply is well functioning.

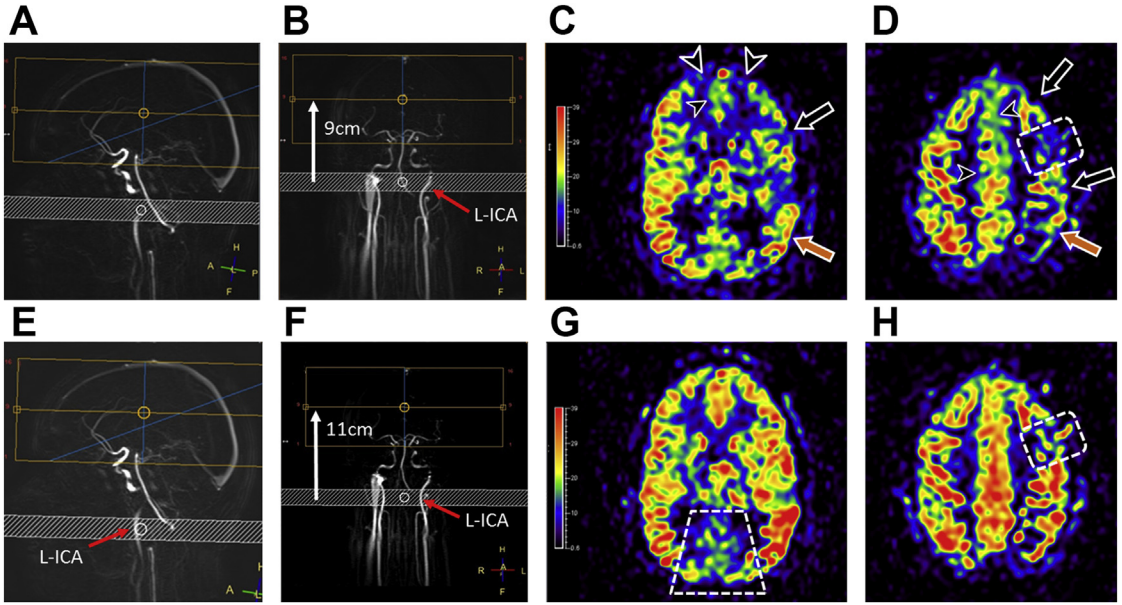

Fig. 18. 3D pseudocontinuous ASL (pCASL) images from a patient with chronic stage of carbon monoxide poisoning. Two consecutive pCASL scans from the same exam are shown in the top row (*A*–*D*) and in the bottom row (*E*–*H*). The sagittal and coronal PCA surveys (*A*, *B* and *E*, *F*) show how pCASL was planned. The yellow box is the imaging volume and below it the striped white slab is the labeling plane. (*C*–*G*) and (*D*–*H*) image pairs show the identical slices of the color cerebral blood flow (CBF) maps. The CBF maps are visualized using the same scale. In the first run the labeling distance was 9 cm (*B*, *white arrow*), in accordance with the recommendation by the 2015 ISMRM consensus paper. Extensive low signal is seen in the left middle cerebral artery (MCA) territory (*black and orange arrows* in *C*, *D*) and in both anterior cerebral artery (ACA) territories (*arrowheads*). On the second run the labeling plane was moved 2cm lower, to achieve a more symmetrical labeling of the carotid arteries. The imaging volume is the same. Most of the "hypoperfused" areas "fill up" and show normal and more symmetric signal. The only remaining true hypoperfusion is in the posterior left frontal lobe, indicated by dashed rectangle in (*D*) and (*H*). The more symmetric and perpendicular ICA labeling has likely led to better labeling efficiency and resulted in higher signal on the left, despite the 2-cm longer labeling distance (11 cm, *white arrow* in *F*). Relatively lower signal is seen in the posterior circulation bilaterally, marked by the white trapezoid in (*G*). This difference between the posterior cerebral artery (PCA) territories and ICA territories is often observed in cases when the PCAs arise from the basilar artery, and may be due to less efficient labeling of blood in the vertebral arteries, or perhaps longer arterial transit time. This phenomenon can be confusing and may be misinterpreted as posterior parietal hypoperfusion. Its clinical importance is that posterior parietal hypoperfusion on ASL has been described in early Alzheimer's disease; therefore, extra attention is needed with regard to anatomic variations when applying ASL in neurodegenerative cases in clinical practice. A unilateral fetal PCA may further complicate the situation, as its territory shows a signal similar to that in ICA territories, whereas the contralateral regular PCA may still show relatively lower signal.

ASL scans individually based on the vascular anatomy. The use of PCA survey images is a quick and effective way to map internal carotid artery anatomy and should always be performed before ASL scans. In the future, artificial intelligence–powered automated vessel labeling will likely be applied to maximize labeling efficiency by mapping the patient's vascular anatomy, identifying the ideal arterial segments, and selectively labeling each vessel with individual labeling planes that are optimized for vessel geometry.

MRI perfusion tends to provide relative, nonquantitative estimates of regional perfusion, as opposed to nuclear medicine or even CT, which has been better at truly quantitative perfusion. Although not yet available commercially, ASL quantification would represent an important clinical advance. Indeed, without this feature, proper interpretation is hampered, which is one area where ASL has to improve to become a widely used clinical technique (**Fig. 19**).

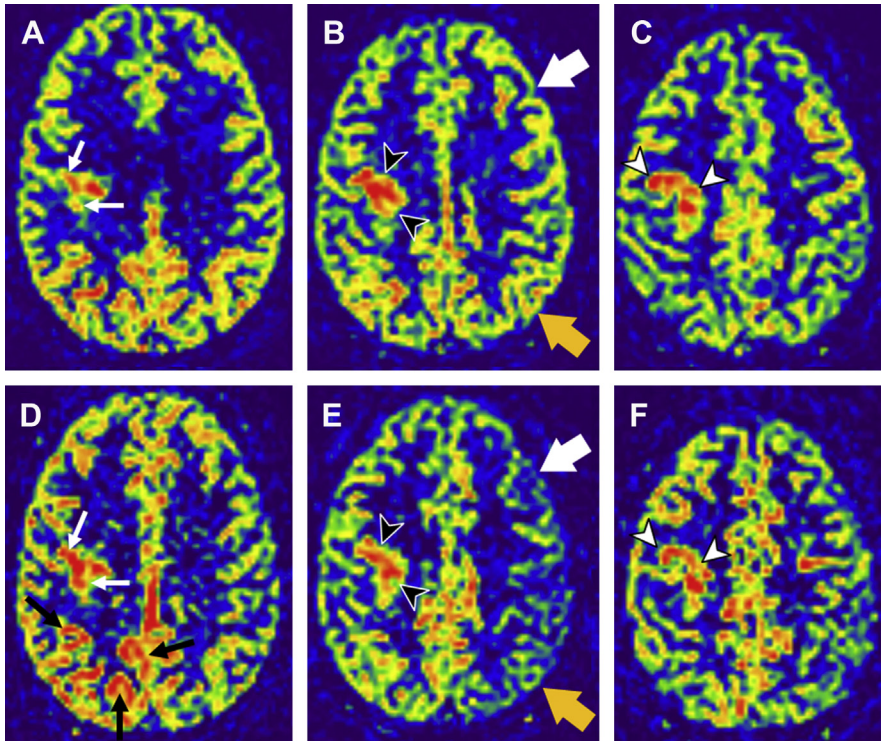

Fig. 19. Serial ASL imaging of an anaplastic astrocytoma. The top row (*A–C*) shows the cerebral blood flow map from the baseline scan; the bottom row (*D–F*) is the follow-up 2 months later, after chemotherapy. (*A–D*), (*B–E*), and (*C–F*) are identical slices. In (*E*) and (*F*) the CBF in the center of the lesion is lower and the extent of the highest perfusion is smaller compared with the baseline images, which might indicate therapeutic response (compare *black and white arrowheads* on the identical slices). However, in (*D*) there is higher CBF compared with baseline (*arrows* in *A* versus *D*). There is similarly higher signal in the right posterior cortical areas (*black arrows* in *D*), suggesting a measurement artifact. On closer look asymmetrical signal distribution is seen with higher signal on the right, most conspicuously on (*D*) and (*E*): compare the signal distribution in the 2 hemispheres in (*A*) and (*B*) (symmetric) versus (*D*) and (*E*) (*black arrows*). The conflict could be resolved by the quantification of ASL, which could eliminate the anatomical bias and operator dependency.

Functional MRI and Spectroscopy, and Quantitative MRI

Functional MRI relies on subtle susceptibility changes related to blood oxygenation. A dynamic 3D T2*-weighted FE sequence is obtained to monitor signal changes pixel by pixel. In the paradigm method, a correlation is drawn between regional signal changes and tasks that stimulate functional regions of the brain. Paradigm fMRI is most used in assessing regions of eloquent brain surrounding brain tumors, and as a replacement for a WADA test. Multiple paradigms are typically used to identify motor and language centers. Special training is required to ensure the patient understands and abides by the task instructions given during the examination. In resting state fMRI (rs-fMRI), inherent correlations between regional oxygenation (activity) changes are used to infer neural network connectivity.[36] Although the postprocessing is complex, the acquisition itself is effectively no different from a conventional MRI from a patient and scan-time perspective.

Proton spectroscopy has been in the sequence arsenal since the early days of MRI. Spectra from individual locations can be displayed, as well as colorized images representing a choice of metabolites, such as *N*-acetyl aspartate (NAA), choline, creatine, lactic acid, and myoinosotol. The normal shape of an magnetic resonance spectroscopy plot follows "Hunter's angle," whereby NAA, creatine, and choline peaks line up in descending order from right to left. The magnetic resonance spectroscopy plot in **Fig. 10** illustrates elevated choline and depressed NAA peaks (inverted Hunter's angle) in a malignant tumor.

New Types of Physiologic Imaging and Amide Proton Transfer

Physiologic MRI of the brain has been an area of research focus since the early 1990s. Structural scans still provide the core of every imaging study, and postprocessing of structural images to obtain tissue volume information can improve clinical insights, as illustrated in **Figs. 20** and **21**. Still, structural imaging tends to show end results of

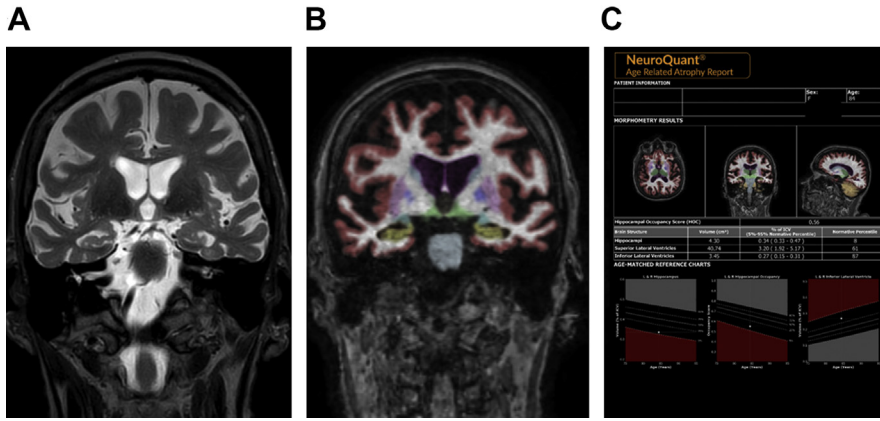

Fig. 20. Coronal T2-weighted image (*A*) shows diffuse enlargement of the frontal and temporal sulci, as well as the body and temporal horns of the lateral ventricles. (*B*) shows the color segmentation of the 3D T1 image in coronal plane, at the same slice position as (*A*). The hippocampi are marked in yellow. The age-related atrophy report (*C*) provides the absolute combined volumes of the hippocampi and lateral ventricles, their proportion in the intracranial volume, and the normative percentile compared with a database of healthy age-matched controls. At the bottom of the report, these values are visualized.

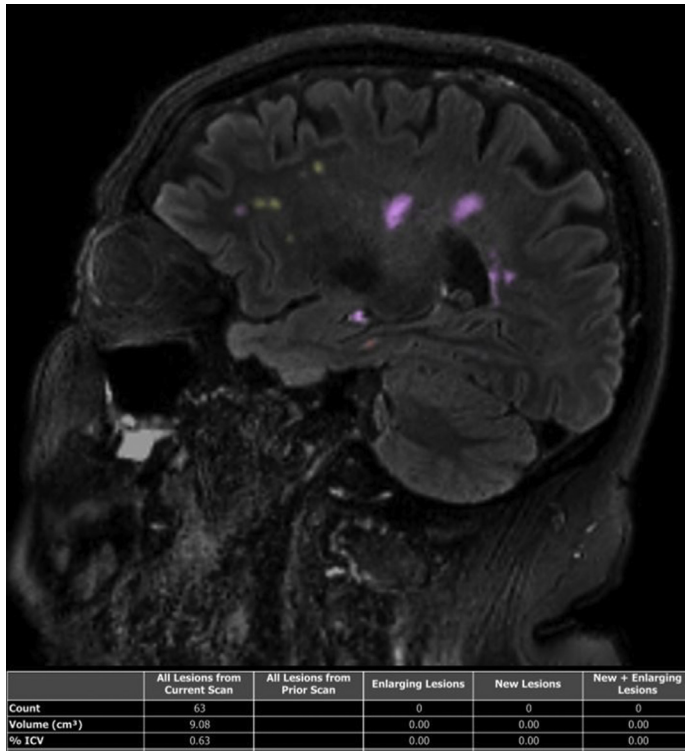

	All Lesions from Current Scan	All Lesions from Prior Scan	Enlarging Lesions	New Lesions	New + Enlarging Lesions
Count	63		0	0	0
Volume (cm³)	9.08		0.00	0.00	0.00
% ICV	0.63		0.00	0.00	0.00

Fig. 21. The automated lesion quantification in multiple sclerosis provides a colored segmentation map of FLAIR hyperintensities and assigns color based on the lesion location. In the report, the lesion distribution and overall lesion volume are shown. On follow-up examinations the difference is also provided, simplifying interpretation and reducing reading time.

pathophysiological changes. Attempts to track the circulation, oxygen extraction, protein metabolism, membrane turnover, and other mechanisms in the brain are intended to reveal disease processes at early stages. As a result, techniques such as perfusion MRI, fMRI, quantitative flow and dynamic studies, magnetic resonance spectroscopy, and DTI have grown in popularity.[37,38]

A relatively new group of physiologic imaging techniques in the clinical research and early clinical implementation is chemical exchange saturation transfer (CEST), whereby magnetization transfer (proton exchange) between a target molecule and water is used to indirectly assess differences in regional distribution of that molecule.[39,40] When a saturation pulse is applied for the target molecule's frequency, the water signal will be reduced proportionally to the proton exchange and this signal change will be visualized on an "asymmetry map." This will replace as a focal intensity change on the CEST image, but is not an absolute measurement of the amount of the substance.

There are multiple different CEST techniques, each specified for a certain molecule (eg, glucose, glycosaminoglycans, amine proton, or creatine).[41,42] Amide proton transfer (APT) is the type of CEST that generates contrast based on the concentration of endogenous mobile proteins and tissue pH.[43] It has been studied in brain tumor diagnostics with promising results: it was shown to discriminate between low-grade and high-grade gliomas,[44] predict isocitrate dehydrogenase status[45] in gliomas, help

guide brain biopsy,[43] differentiate between true progression and pseudoprogression,[46] distinguish between metastasis and glioblastoma,[47] and explored in other areas such as hypoxic ischemic injury.[48]

APT imaging is available commercially, and relative to spectroscopy is very simple to run. Lesions appear as an obvious focal spot against a background of homogeneous normal tissue that does not exhibit conventional resolution and contrast variations of classic MRI scans (**Figs. 22** and **23**). It is noteworthy that even the ventricles do not stand out because the water signal is distributed evenly.

Applications for APT are still under investigation. More studies are needed to fully understand its diagnostic power in tumor diagnostics and therapy monitoring. Also, it is an EPI sequence and cannot be used in the posterior fossa or on the skull base in most cases. It often has prominent EPI artifacts along the skull and postoperative areas (which may render it less useful in tumor cases), and intravascular artifacts may cause uncertainty in interpretation as well. Based on early experience with serial imaging, its reproducibility is variable. Its variability to pH changes can be a weakness and a strength. Clinical studies and further engineering work are expected to clarify solutions to many of these issues.

APT is a good candidate to become a clinically useful technique. It already has a role in tumor imaging. It is unlikely that APT will remain the only CEST player in clinical practice given its physiological target substrate represents a narrow focus. Rather,

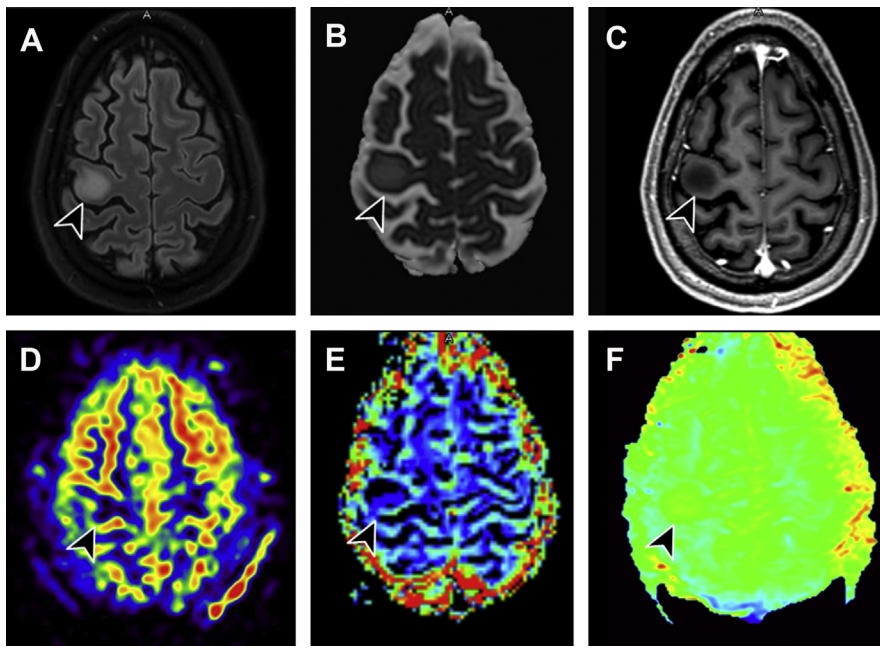

Fig. 22. Multiparametric imaging of a low-grade glioma with brain perfusion and amide proton transfer (APT) imaging. The infiltrative tumor is located in the right precentral gyrus (*black arrowhead*), exhibiting hyperintense signal on FLAIR (*A*), increased diffusion on ADC (*B*), and no abnormal contrast enhancement (*C*). The 3D pCASL-derived CBF map (*D*) and the DSC-derived rCBV map (*E*) show no increased perfusion compared with the normal parenchyma. Subtle signal increase is seen on the APT (*F*, *arrowhead*). The physiologic findings are consistent with a low-grade tumor and are in accordance with the structural scans.

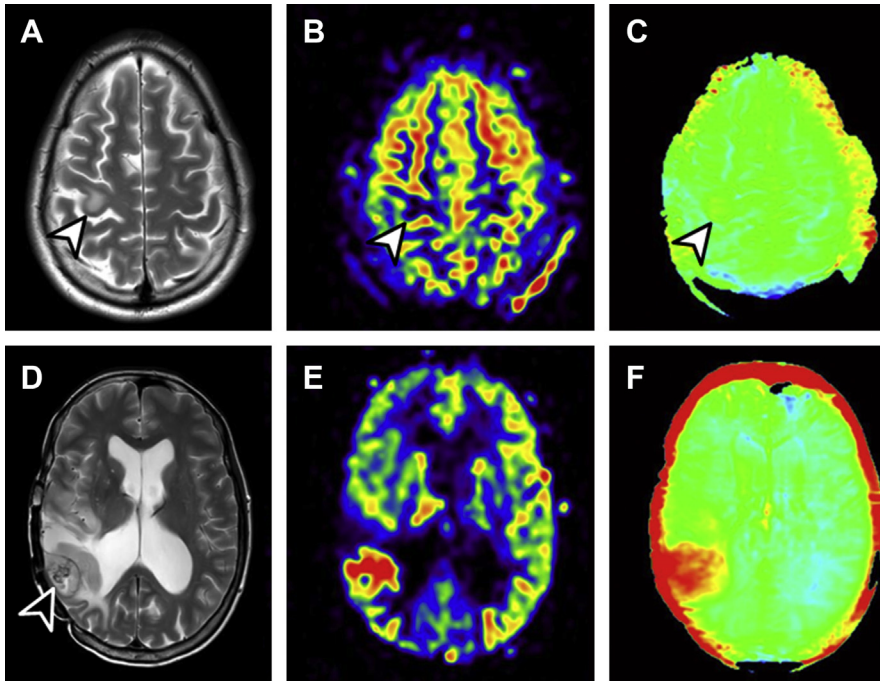

Fig. 23. Multiparametric imaging of brain tumors with arterial spin labeling and amide proton transfer (APT). The top row shows a low-grade glioma in the right precentral gyrus (*white arrowhead*) with homogeneous high T2 signal (*A*), without increased CBF on the 3D pCASL scan (*B*) and without abnormal signal increase on 3D APT (*C*). The bottom row demonstrates a recurrent glioblastoma with heterogeneous structure on T2 (*D*, *black arrowhead*) and markedly elevated CBF (*E*) as well as APT (*F*) signal.

it may eventually be recognized as the first of a bigger CEST portfolio. A clinically useful and versatile tool of the future may be a CEST map: a sequence that acquires and combines different CEST contrasts (amide proton, glucose, etc), providing a comprehensive picture of brain metabolism, which could be used in conjunction with other physiologic techniques and perhaps even tailored for specific diseases.

Fast Imaging Methods

An important limitation of MRI is its inherently long scan time. Although diagnostic insight is improved by maximizing signal-to-noise ratio, resolution, and obtaining multiple tissue contrasts and views, the total scan time will increase. As a result, motion artifact becomes more likely as patients become uncomfortable, tolerance to complete the study is reduced, and affordability becomes a factor as scanner capacity decreases. These practical constraints limit the acceptable duration of a scan. To overcome this constraint, MRI technology is increasingly integrating new algorithms and hardware with innovations in data science and artificial intelligence. As such innovations are implemented, new parameters, complexities, and artifacts are inevitably introduced, which will require clinical optimization, education, and practical adjustments.

Compressed sensing and spiral imaging are two fast MRI methods that are currently the subject of extensive research and development. Spiral imaging is not yet

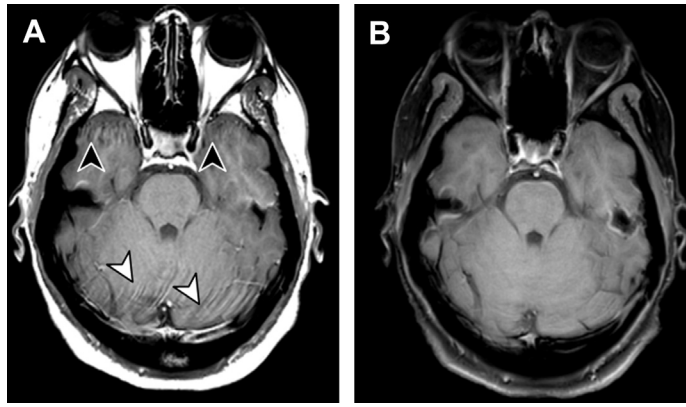

Fig. 24. Cartesian T1 spin echo (*A*) shows typical flow artifacts in phase direction, originating from the transverse sinuses (*white arrowheads*) and from the internal carotid arteries (*black arrowheads*). These artifacts are completely missing from the spiral acquisition (*B*), creating a clearer image of the cerebellum, the temporal poles, and the parasellar regions.

commercially available as of the date of this writing, but research has shown promising results in T1-weighted brain and spine imaging, DWI, ASL, and TOF MRA.[49–56] Compared with standard TSE or SE scans, it can achieve higher signal-to-noise ratio under shorter scan time, dramatically reduce classic flow artifacts, and has inherent fat suppression using the Dixon method (**Figs. 24–26**). These examples also

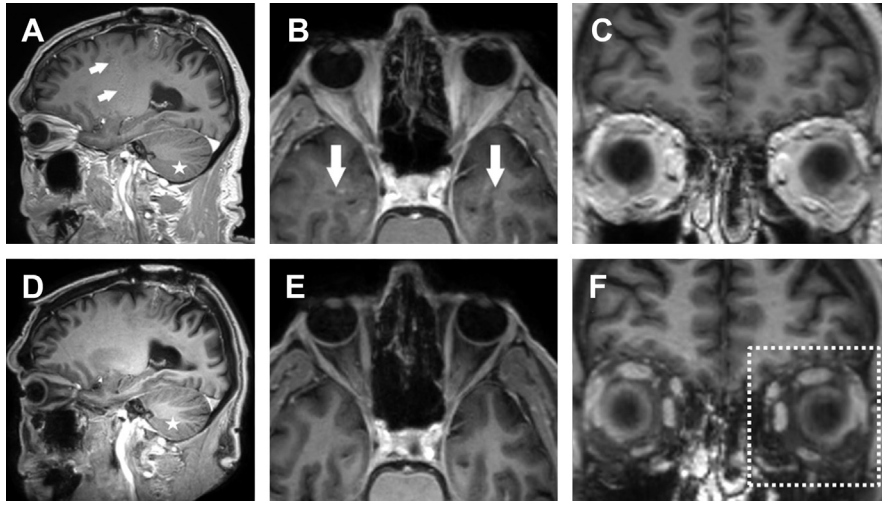

Fig. 25. Comparison of Cartesian (*A–C*) and spiral (*D–F*) contrast-enhanced 3D T1 TFE scans. The spatial resolution is 0.94 mm isotropic for both scans. The spiral is shorter (3:30 min vs 4:45 min), has higher SNR (*A and D*, *asterisk*) and flow artifact mitigation (*A and B*, *arrows*), resulting in higher image quality. It also uses Dixon for fat suppression, which can be exploited in many clinical scenarios, such as the imaging of the orbits, which normally requires additional fat-saturated scans before and after administration of GBCA. By using spiral 3D T1 the fat-suppressed orbital images can be reconstructed from the brain 3D dataset (*F*, *dashed rectangle*), eliminating the need for running additional sequences. Thus, a significant amount of time can be saved in clinical workflow.

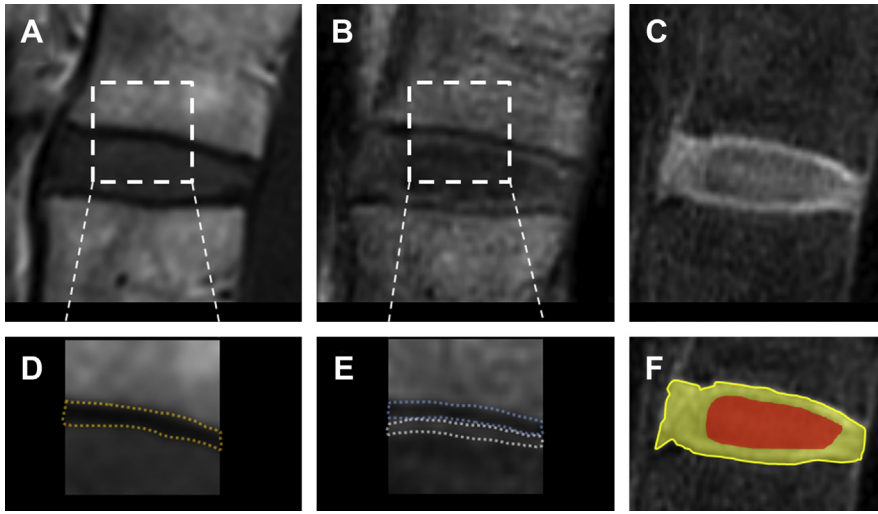

Fig. 26. Comparison of a standard Cartesian T1-weighted scan (*A*) and a spiral T1-weighted research scan using Dixon technique (*B*, *C*). In (*A*) the endplate appears as one dark band, while on the in-phase spiral image (*B*) it is separated into an upper darker and lower brighter layer, which may represent the real endplate and the annulus fibrosus, respectively. These structures are blown up and highlighted in (*D*) and (*E*); blue dotted line delineates the endplate and white dotted line the annulus on (*E*). The water-only image of spiral scan (*C*) shows an outer brighter and a central darker component, likely representing the annulus fibrosus and the nucleus pulposus of the intervertebral disc. These are highlighted in yellow and red in (*F*). This more detailed image of the intervertebral disc and the vertebral body may provide useful diagnostic information in the early phase of the evolution of degenerative spine disease, as it may visualize annular tear, endplate changes, and early formation of disc herniation.

demonstrate that fast or efficient imaging protocols can either increase the capacity of an MRI or permit additional scrutiny in the same patient time slot. A current disadvantage of spiral imaging is that image blurriness and EPI artifacts must yet be overcome.

Compressed sensing is currently offered commercially. It operates with a sparse data sampling and iterative reconstruction methodology that mimics newer CT reconstruction algorithms, and has been shown to produce 25% to 30% reduction in scan time under certain conditions (**Figs. 27–29**).[57,58] However, compressed sensing comes with a slight change of image character that will require user acclimation. It cannot be applied to EPI scans, and to date requires individual protocol optimization to maintain image quality. Because its speedup relies on eliminating information redundancy in data acquisition, its performance relies on the greater signal-to-noise ratio achieved at higher field strength MRI systems and efficient coil technology. Compressed sensing is well positioned to reduce scan time without compromising diagnostic quality of high-resolution images. Ongoing development and clinical optimization are expected to further reduce examination time and mitigate artifacts.

It is likely that a combination of different approaches, rather than any of these individual techniques alone, will be needed to make dramatic improvements in clinical MRI scan times. Today, a typical brain examination consists of 5 or more structural scans and lasts for 15 to 30 minutes. A full spine and brain examination can be as long as 1 hour. The real difference will be when a brain MRI examination becomes as fast as a brain CT (ie, less than 1 minute) without sacrificing image quality. This lofty goal does not seem unrealistic given the strong interest and current state of research

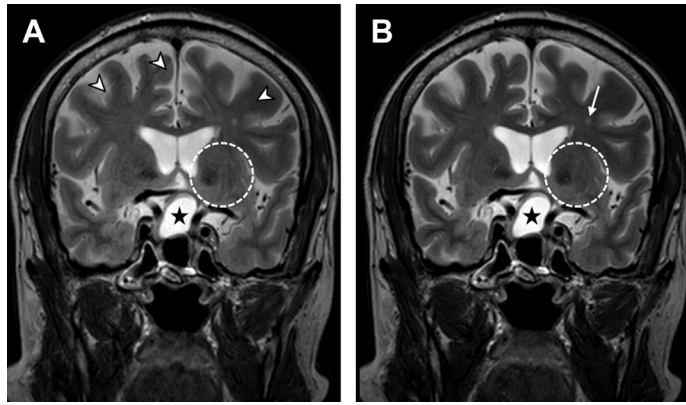

Fig. 27. Comparison of sensing (SENSE) and compressed sensing (C-SENSE) accelerated T2-weighted images. (*A*) is acquired using regular SENSE, with 2:30 min scan time. (*B*) uses C-SENSE, with 1:26 min scan time. Mild motion artifacts are seen in (*A*) (*arrowheads*), which are reduced in (*B*). The overall appearance of the basal ganglia is more consistent in (*B*) (compare the circled areas). The size and signal characteristics of the small white matter lesion in the left frontal lobe is unchanged (*B*, *white arrow*). The intrasellar-suprasellar cystic abnormality (*asterisk*) and the parasellar structures show the same signal and edge definition on the 2 scans. The overall clinical diagnostic utility is not affected by using C-SENSE.

in this area. Such increased speed will require concomitant innovations in practical implementation, including how to move patients in and out efficiently, reading a higher volume of MRI examinations, quality control, and new hardware that may be required to support the new workflow. It is worth noting that although the 1-minute high-

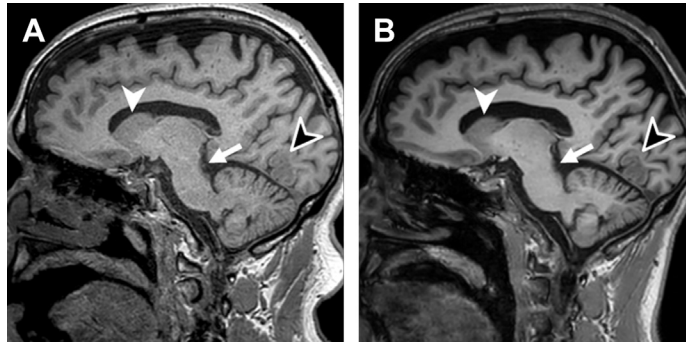

Fig. 28. Comparison of SENSE and C-SENSE accelerated 3D T1 (MPRAGE) images. (*A*) 3D T1 with SENSE acceleration (SENSE factor = 2.2), 0.9 mm isotropic voxels, with a scan time of 4:18 min. (*B*) 3D T1 with C-SENSE acceleration (C-SENSE factor = 3.5), 1 mm isotropic voxels, and scan time of 3:02 min. Image denoising applied by the C-SENSE algorithm is apparent in (*B*) in white matter resulting in a generally better gray-white contrast, which makes the occipital abnormality easier to detect (*black arrowhead*). However, edges in (*B*) are less sharp compared with (*A*), as seen on the superior border of the caudate nucleus (*white arrowhead*), along the posterior border of the pons (*arrow*), and in the cortex. This may have resulted from the slightly larger voxel size and from the iterative image reconstruction used for denoising in C-SENSE. In this regard the image quality of C-SENSE MRI images are similar to computed tomographic images that are reconstructed with iterative algorithms: the images appear smoother and have a "plastic-like" character.

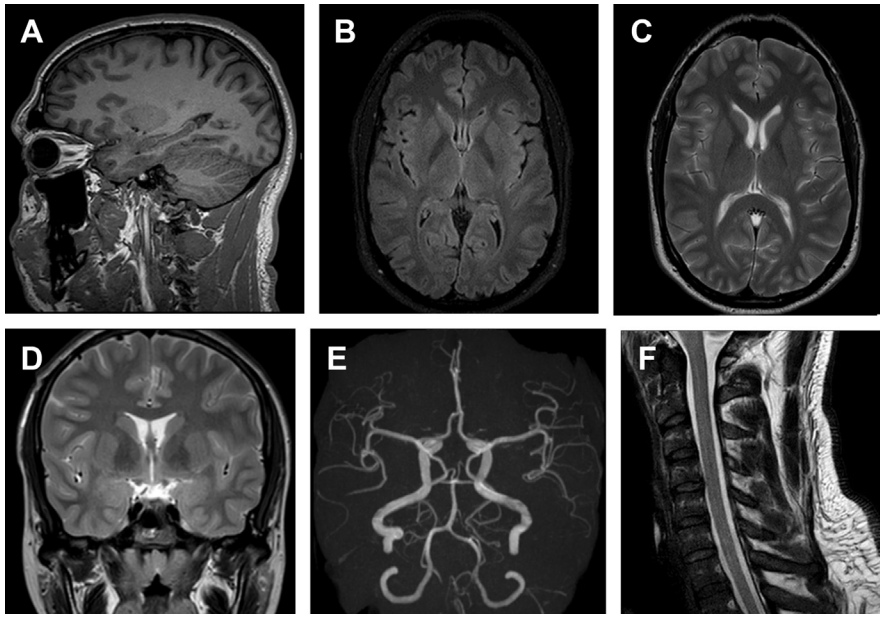

Fig. 29. C-SENSE accelerated head and spine imaging in a rapid headache protocol on 3T. The total exam length is 16:07 min with the following individual scan times: sagittal 3D T1 (*A*): 3:37 min; axial 3D FLAIR (*B*): 4:00 min; axial 2D T2 TSE (*C*): 1:24 min; coronal 2D TSE (*D*): 1:26 min; 3D TOF MRA (*E*): 3:46 min; sagittal 2D TSE of the cervical spine (*F*): 1:54 min.

resolution MRI examination does not yet exist in routine practice, some of the listed new techniques already save substantial scan time that allows for additional physiologic data to be collected in conventional time slots; this benefit may have an even greater positive impact on neuroradiology than the sheer exam time reduction.

SUMMARY

The review of some of the clinical and fundamental principles of MRI presented in this article serves as only a basic foundation in this increasingly complex field. More rigorous study of neuroimaging is vital for all neurologists, at a minimum to understand the language and logic of neuroradiology, thus improving communication and patient care. It is increasingly important for the ordering neurologist to understand advantages and disadvantages of routine and specialty sequences, and to be able to perform at least cursory review of images. Furthermore, a wide spectrum of additional advantages occurs as training and experience in imaging interpretation increases.[3] With its disciplined process of relating lesion visualization to symptoms, MRI skills arguably make for better neurologists. Certain subspecialties, such as stroke specialists, critical care neurologists, interventional neurologists, and practitioners who use teleneurology tend to rely their own image review to make treatment decisions. Neuroimaging is a logical component of comprehensive neuroscience group practices, and neurologists trained in neuroimaging can offer tremendous value in such organizations.[59]

Ultimately, it takes time to develop an in-depth understanding of technical aspects of imaging, translate physiologic and pathologic processes into pixels through those

physical principles, and integrate this new knowledge into clinical scenarios. There are precedents and resources for neurologists seeking to develop more advanced skills, including rotations, preceptorships, remote didactics, professional conferences, and formal fellowship programs through societies such as the American Society of Neuroimaging, the American Academy of Neurology, the American Society of Neuroradiology, the Radiologic Society of North America, and the United Council for Neurologic Subspecialties.

REFERENCES

1. Viallon M, Cuvinciuc V, Delattre B, et al. State-of-the-art MRI techniques in neuroradiology: principles, pitfalls, and clinical applications. Neuroradiology 2015; 57(5):441–67.
2. Fritz JV. Neuroimaging trends and future outlook. Neurol Clin 2014;32(1):1–29.
3. Mechtler L, Fritz J. Why neuroimaging plays a critical role in shaping the future of neurology. Pract Neurol 2016;16:17–20.
4. Fritz JV. What neurologists need to know about MRI sequences. Paper presented at: American Academy of Neurology Annual Meeting. Philadelphia, April 30, 2014.
5. Mamourian A, Lembo J, Mamourian M. Top ten MR artifacts. Oxford (England): Radiology Boards Prep; 2015.
6. Mamourian AC. Practical MR physics and case file of MR artifacts and pitfalls. Oxford (England): Oxford Univesity Press; 2010.
7. Hornack JP. The basics of MRI. 2019. Available at: https://www.cis.rit.edu/htbooks/mri/. Accessed April 22, 2019.
8. The MRI Registry Review Program. Medical imaging consultants. 2019. Available at: http://www.micinfo.com/courses/mrrrp/index.xml?ss=course_detail. Accessed April 22, 2019.
9. Currie S, Hoggard N, Craven IJ, et al. Understanding MRI: basic MR physics for physicians. Postgrad Med J 2013;89:209–23.
10. Shellock F. MRISafety.com. 2019. Available at: http://www.mrisafety.com/. Accessed April 24, 2019.
11. Korutz AW, Obajuluwa A, Lester MS, et al. Pacemakers in MRI for the neuroradiologist. AJNR Am J Neuroradiol 2017;38(12):2222–30.
12. Ramalho J, Semelka RC, Ramalho M, et al. Gadolinium-based contrast agent accumulation and toxicity: an update. AJNR Am J Neuroradiol 2016;37(7):1192–8.
13. Chehabeddine L, Al Saleh T, Baalbaki M, et al. Cumulative administrations of gadolinium-based contrast agents: risks of accumulation and toxicity of linear vs macrocyclic agents. Crit Rev Toxicol 2019;1–18. https://doi.org/10.1080/10408444.2019.1592109.
14. Weiner SL, Ru R, Javan R, et al. Health care economics: a study guide for neuroradiology fellows, part 1. AJNR Am J Neuroradiol 2018;39(1):2–9.
15. Buethe J, Nazarian J, Kalisz K, et al. Neuroimaging wisely. AJNR Am J Neuroradiol 2016;37(12):2182–8.
16. Appropriate use criteria. Centers for Medicare and Medicaid Services. 2016. Available at: www.cms.gov/Medicare/Quality-Initiatives-Patient-Assessment-Instruments/Appropriate-Use-Criteria-Program/index.html. Accessed September 21, 2019.
17. Bernstein MA, Huston J, Ward HA. Imaging artifacts at 3.0T. J Magn Reson Imaging 2006;24:735–46.

18. Haake EM, DelProposto ZS, Chaturvedi S, et al. Imaging cerebral amyloid angiopathy with susceptibility-weighted imaging. AJNR Am J Neuroradiol 2007;28(2):316–7.
19. McNamara C, Sugrue G, Murray B, et al. Current and emerging therapies in multiple sclerosis: implications for the radiologist, part 2—surveillance for treatment complications and disease progression. AJNR Am J Neuroradiol 2017;38(9):1672–80.
20. Arevalo O, Riascos R, Rabiei P, et al. Standardizing magnetic resonance imaging protocols, requisitions, and reports in multiple sclerosis: an update for radiologist based on 2017 magnetic resonance imaging in multiple sclerosis and 2018 Consortium of Multiple Sclerosis Centers Consensus Guide. J Comput Assist Tomogr 2019;43(1):1–12.
21. Fernanda RLC, Hygino da Cruz LC Jr, Doring M, et al. Diffusion-weighted imaging and demyelinating diseases: new aspects of an old advanced sequence. Am J Roentgenol 2014;202(1):W34–42.
22. Davoudi Y, Foroughipour M, Torabi R, et al. Diffusion weighted imaging in acute attacks of multiple sclerosis. Iran J Radiol 2016;13(2):e21740.
23. Osborn AG, Salzman KL, Jhaveri MD, et al. Diagnostic imaging: brain. 3rd edition. Philadelphia (PA): Elsevier; 2015.
24. Ptak T, Sheridan RL, Rhea JT, et al. Cerebral fractional anisotropy score in trauma patients: a new indicator of white matter injury after trauma. Am J Roentgenol 2003;181(5):1401–7.
25. Edlow BL, Copen WA, Izzy S, et al. Longitudinal diffusion tensor imaging detects recovery of fractional anisotropy within traumatic axonal injury lesions. Neurocrit Care 2016;24(3):342–52.
26. Li XH, Wu F, Zhao F, et al. Fractional anisotropy is a marker in early-stage spinal cord injury. Brain Res 2017;1672:44–9.
27. Haller S, Etienne L, Varoquaux AD, et al. Imaging of neurovascular compression syndromes: trigeminal neuralgia, hemifacial spasm, vestibular paroxysmia, and glossopharyngeal neuralgia. AJNR Am J Neuroradiol 2016;37(8):1384–92.
28. Besta R, Shankar YU, Kumar A, et al. MRI 3D CISS- a novel imaging modality in diagnosing trigeminal neuralgia - a review. J Clin Diagn Res 2016;10(3):ZE01–3.
29. Yamada S, Tsuchiya K, Bradley W, et al. Current and emerging MR imaging techniques for the diagnosis and management of CSF flow disorders: a review of phase-contrast and time–spatial labeling inversion pulse. AJNR Am J Neuroradiol 2015;36(4):623–30.
30. Delfaut EM, Beltran J, Johnson G, et al. Fat suppression in MR imaging: techniques and pitfalls. Radiographics 1999;19:373–82.
31. Pokomey AL, Chia JM, Pfeifer CM, et al. Improved fat-suppression homogeneity with mDIXON turbo spin echo (TSE) in pediatric spine imaging at 3.0T. Acta Radiol 2017;58(11):1386–94.
32. Lapointe E, Li DKB, Traboulsee AL, et al. What have we learned from perfusion MRI in multiple sclerosis? AJNR Am J Neuroradiol 2018;39(6):994–1000.
33. Gaddikeri S, Gaddikeri RS, Tailor T, et al. Dynamic contrast-enhanced MR imaging in head and neck cancer: techniques and clinical applications. AJNR Am J Neuroradiol 2016;37(4):588–95.
34. Alsop DC, Detre JA, Golay X, et al. Recommended implementation of arterial spin labeled perfusion MRI for clinical applications: a consensus of the ISMRM perfusion study group and the European consortium for ASL in dementia. Magn Reson Med 2015;73(1):102–16.

35. Li Y, Mao D, Li Z, et al. Cardiac-triggered pseudo-continuous arterial-spin-labeling: a cost-effective scheme to further enhance the reliability of arterial-spin-labeling MRI. Magn Reson Med 2018;80(3):969–75.
36. Lv H, Wang Z, Tong E, et al. Resting-state functional MRI: everything that nonexperts have always wanted to know. AJNR Am J Neuroradiol 2018;39(8):1390–9.
37. Zhou M, Scott J, Chaudhury B, et al. Radiomics in brain tumor: image assessment, quantitative feature descriptors, and machine-learning approaches. AJNR Am J Neuroradiol 2018;39(2):208–16.
38. Zaharchuk G, Gong E, Wintermark M, et al. Deep learning in neuroradiology. AJNR Am J Neuroradiol 2018;39(10):1776–84.
39. Ward KM, Aletras AH, Balaban RS. A new class of contrast agents for MRI based on proton chemical exchange dependent saturation transfer (CEST). J Magn Reson 2000;143:79–87.
40. Zhou J, van Zijl PC. Chemical exchange saturation transfer imaging and spectroscopy. Prog Nucl Magn Reson Spectrosc 2006;48:109–36.
41. Jones KM, Pollard AC, Pagel MD. Clinical applications of chemical exchange saturation transfer (CEST) MRI. J Magn Reson Imaging 2018;47(1):11–27.
42. Pankowska A, Kochalska K, Łazorczyk A, et al. Chemical exchange saturation transfer (CEST) as a new method of signal obtainment in magnetic resonance molecular imaging in clinical and research practice. Pol J Radiol 2019;84:e147–52.
43. Shanshan J, Eberhartc C, Zhanga Y, et al. Amide proton transfer-weighted MR image-guided stereotactic biopsy in patients with newly diagnosed gliomas. Eur J Cancer 2017;83:9–18.
44. Choi YS, Ahn SS, Seung-Koo L, et al. Amide proton transfer imaging to discriminate between low- and high-grade gliomas: added value to apparent diffusion coefficient and relative cerebral blood volume. Eur Radiol 2017;27:3181–9.
45. Jiang S, Zou T, Eberhart CG, et al. Predicting IDH mutation status in grade ii gliomas using amide proton transfer-weighted(APTw) MRI. Magn Reson Med 2017;78:1100–9.
46. Ma B, Blakeley JO, Hong X, et al. Applying amide proton transfer-weighted MRI to distinguish pseudoprogression from true progression in malignant gliomas. J Magn Reson Imaging 2016;44:456–62.
47. Yu H, Lou H, Zou T, et al. Applying protein-based amide proton transfer MR imaging to distinguish solitary brain metastases from glioblastoma. Eur Radiol 2017;27(11):4516–24.
48. Zheng Y, Wang X. The applicability of amide proton transfer imaging in the nervous system: focus on hypoxic-ischemic encephalopathy in the neonate. Cell Mol Neurobiol 2018;38:797–807.
49. Li Z, Schär M, Wang D, et al. Arterial spin labeled perfusion imaging using three-dimensional turbo spin echo with a distributed spiral-in/out trajectory. Magn Reson Med 2016;75(1):266–73.
50. Ahn CB, Kim JH, Cho ZH. High-speed spiral-scan echo planar NMR imaging-I. IEEE Trans Med Imaging 1986;5(1):2–7.
51. Meyer CH, Hu BS, Nishimura DG, et al. Fast spiral coronary artery imaging. Magn Reson Med 1992;28(2):202–13.
52. Pipe JG, Robison RK. Simplified signal equations for spoiled gradient echo MRI. Paper presented at: Proceedings of the 18th Annual Meeting of ISMRM, Stockholm, 2010.
53. Nishimura DG, Irarrazabal P, Meyer CH. A velocity k-space analysis of flow effects in echo-planar and spiral imaging. Magn Reson Med 1995;33(4):549–56.

54. Wang D, Zwart NR, Pipe JG. Joint water-fat separation and deblurring for spiral imaging. Magn Reson Med 2018;79(6):3218–28.
55. Li Z, Karis JP, Pipe JG. A 2D spiral turbo-spin-echo technique. Magn Reson Med 2018;80(5):1989–96.
56. Li Z, Hu HH, Miller JH, et al. A spiral spin-echo MR imaging technique for improved flow artifact suppression in T1-weighted postcontrast brain imaging: a comparison with cartesian turbo spin-echo. AJNR Am J Neuroradiol 2016; 37(4):642–7.
57. Sartoretti T, Reischauer C, Sartoretti E, et al. Common artefacts encountered on images acquired with combined compressed sensing and SENSE. Insights Imaging 2018;9:1107–15.
58. Worters P, Sung K, Stevens K, et al. Compressed-sensing multi-spectral imaging of the post-operative spine. J Magn Reson Imaging 2013;37(1):243–8.
59. Fritz JV. The practice of neuroimaging within a neurology office setting. Neurol Clin Pract 2013;3(6):501–9.